Analytical model for laterally loaded pile groups in layered sloping soil

Hemel, Mart Jan; Korff, Mandy; Peters, Dirk Jan

DOI
10.1016/j.marstruc.2022.103229

Publication date
2022

Document Version
Final published version

Published in
Marine Structures

Marine Structures 84 (2022) 103229

Contents lists available at ScienceDirect

Marine Structures

journal homepage: www.elsevier.com/locate/marstruc

Analytical model for laterally loaded pile groups in layered sloping soil

Mart-Jan Hemel [a,b,*], Mandy Korff [a,c], Dirk Jan Peters [a,d]

[a] Faculty of Civil Engineering and Geoscience, Delft University of Technology, Delft, 2628, CN, Netherlands
[b] Amsterdam Institute for Advanced Metropolitan Solutions (AMS), Amsterdam, 1018, JA, Netherlands
[c] Deltares, P.O. Box 177, 2600, MH, Delft, the Netherlands
[d] Department of Hydraulic Structures, Royal HaskoningDHV, Rotterdam, 3068, AX, Netherlands

ARTICLE INFO

Keywords:
Laterally loaded piles
Layered soil
Sloping soil
Brinch hansen
Ménard stiffness
Strain wedge model

ABSTRACT

The historic canal wall structures in many Northern European cities have been built as masonry walls on a timber deck founded on timber piles. For analysis of the resistance of those structures and assessment of their remaining service life, suitable and accurate calculation models are needed. Thereto an analytical method was developed for modelling laterally loaded pile groups in layered sloping soil. In the proposed method, the bending of a pile, which is subjected to a lateral load and axial load, is described by a beam on a Winkler elastic foundation in which the soil behaviour is represented by a series of independent *p-y* springs, idealized with a bilinear elastic-perfect-plastic approximation. The plastic limit was computed with Brinch Hansen ultimate soil resistance and the elastic soil response by the Ménard stiffness. The plastic limit was corrected for each depth, based on the reduction of the passive soil wedge due to pile group effects and the presence of a sloping surface. The analytical model was calibrated and validated with three field experiments, one full-scale lateral load test of a 3 × 5 pile group in soft clays and silts (Snyder, 2004), one full scale lateral load test of a single pile located on a slope in layered soils (Mirzoyan, 2007) and one small scale lateral load test of a single pile located near a slope in sand (Abdelhalim et al., 2020). The proposed method can adequately predict bending moment distributions and pile deflections and in addition, a good consistency between the analytical model and experimental tests was observed. The method is very fast, making it suitable for probabilistic, Monte Carlo type, simulations and reliability updating to determine the probability of failure of quay walls or other structures with horizontally loaded piles.

1. Introduction

Piled structures are often subjected to significant lateral loads. In historic structures, the use of inclined piles was not common and lateral loads were resisted by installing a matrix of vertical piles. Examples of such loading situations can be found in a variety of structures [1]. In offshore structures, waves on platforms, berthing vessels on jetties, floating ice on piers [2] and onshore structures, strong winds on high rise buildings or break and acceleration forces on bridge abutments, earth pressures in soil retaining structures and earthquakes can cause high horizontal forces on pile foundations. When the intermediate distance between piles becomes smaller than ten diameters, group effects, generally referred to as pile-soil-pile interaction become significantly relevant [3].

* Corresponding author. Faculty of Civil Engineering and Geoscience, Delft University of Technology, Delft, 2628, CN, Netherlands.
E-mail address: m.hemel-1@tudelft.nl (M.-J. Hemel).

https://doi.org/10.1016/j.marstruc.2022.103229
Received 31 March 2021; Received in revised form 18 February 2022; Accepted 22 March 2022
Available online 27 April 2022

Laterally loaded pile groups are often found below quay walls. The specific application in this paper relates to historic quay walls in the city centre of Amsterdam. In Amsterdam, the driving of long timber piles (around 12 m) to support quay walls started at the end of the 16th century [4]. Large expansion projects with timber piles were already under development in the 17th and 18th centuries culminating in the late 19th and early 20th century when many Dutch cities expanded [5]. Not surprisingly, these very old quay walls are in a poor condition and may have reached the end of their service life, which in some cases even leads to quay wall collapse [6]. The municipality of Amsterdam is facing a huge task in replacing over 200 km of quay wall of which 135 km has moderated to high risk of collapsing [7]. The structural behaviour of these existing structures is still largely uncharted territory. In practice, it is difficult to prove that these quay walls are safe, or even stable based on the current state of the art models. Because an important part of the uncertainty lies in soil and structural input data, there is clear potential for improving the analysis methods of the old quay walls to prevent these have to be replaced on a large scale and within a short period of time.

One of the possibilities to reduce uncertainties and to get a more accurate understanding of the structural safety, is the application of reliability updating. Information on engineering systems through monitoring, direct observations or measurements of system performances can be used to update the system reliability estimate [8]. However, reliability updating, also known as Bayesian updating, requires fast computational time [9]. Accurate modelling of pile-soil-pile interaction is often accompanied by a considerable computational effort due to the complex nature of the problem. To address this challenge, this paper proposes a fast but accurate method to model the response of laterally loaded pile groups of quay walls. The method is applied to historical quay walls in Amsterdam.

An old poster with cross-sectional drawings of historical quay wall structures can be seen in Fig. 1. The quay wall construction consists of a brick cantilever wall on a timber deck supported by three to six timber pile rows. In many cases, the piles are situated on a downwards sloping canal bed. On top of the timber deck, behind the gravity wall, a layer of fill is present on which roads, parking lots, pedestrian paths and even trees are located. Recently a quay wall in Rotterdam, which has a similar configuration as the quay walls in Amsterdam, was removed and excavated until the timber deck level which can be seen in Fig. 2. The pile rows plus support beams of the deck can be observed as well as the start of the slope in which the piles are located. Horizontal earth pressures from behind the quay

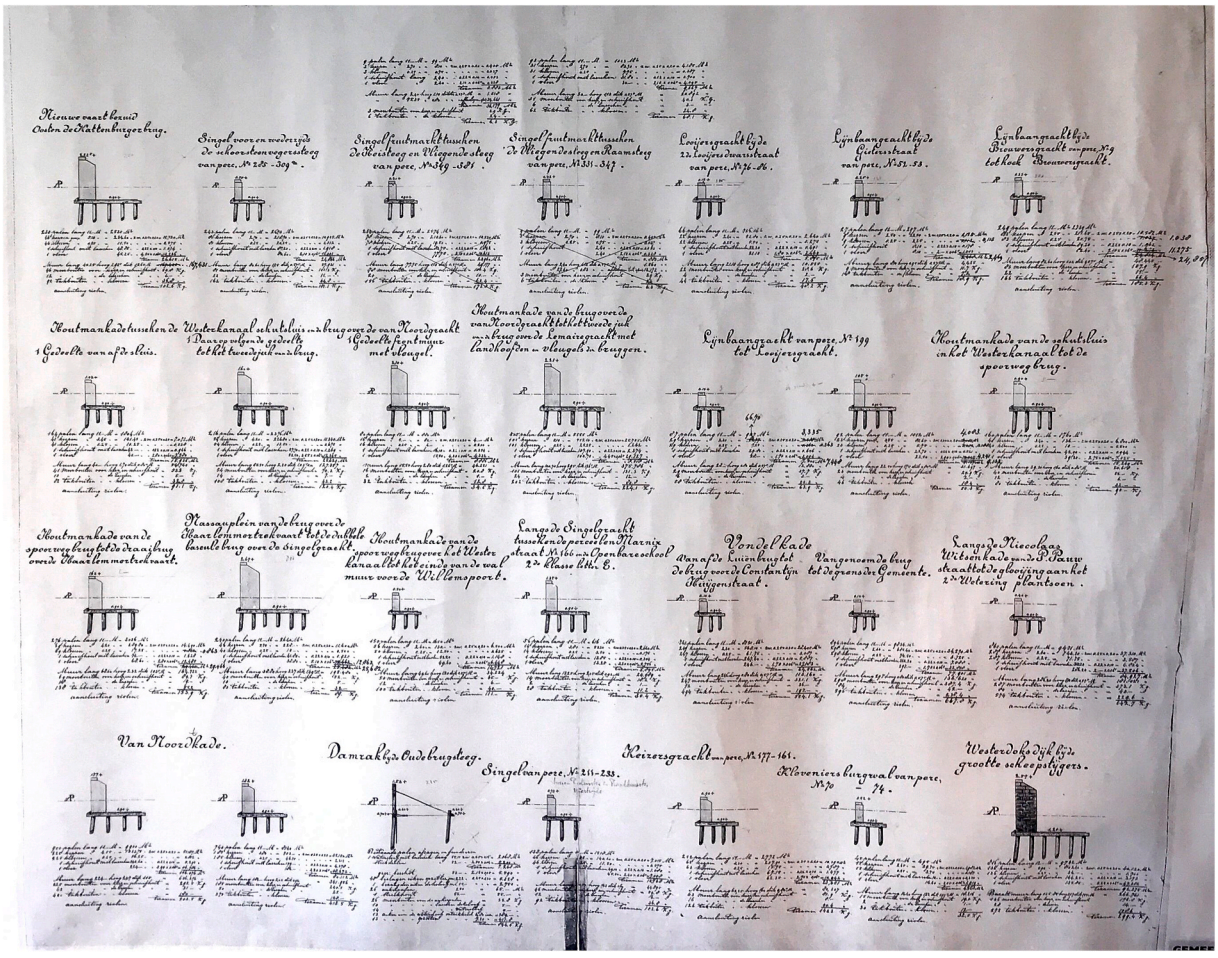

Fig. 1. Documentation of historical quay walls in the city centre of Amsterdam. Source: Archive of Gemeente Amsterdam.

wall cause a lateral load on the pile caps.

The response of a laterally loaded single pile is a complicated soil-structure interaction problem for which reliable methods, to capture the lateral response, have been developed in the past decades. One of the first methods to analyse laterally loaded piles is the ultimate lateral resistance model of Blum [10] in which passive soil resistance is used to find an equilibrium of the pile. This ultimate strength method was improved by Brinch Hansen [11] who made it possible to analyse piles in layered cohesive and granular soils. These ultimate limit state methods fail to predict the deformation and force distributions of the pile. Various methods to predict bending moments, deflections and soil stresses are developed over time. In most of these methods, the pile is modelled as a beam on elastic foundation (BEF). There are many approaches to describe the soil behaviour but for the majority, globally two types can be identified; spring models and continuum models [12].

In the first type of models, the soil behaviour is represented by a series of independent (non)linear springs. The method of Brom [13] used the theory of subgrade reaction to compute the lateral deflections, the ultimate lateral resistance and moment distributions. Matlock [14] proposed the *p-y* curve method which can conveniently take nonlinear behaviour and non-homogeneity property of soil into account. The many *p-y* curves that are developed over time are based on empirical curve fitting from full-scale experiments [15], centrifuge model tests [16] and finite element modelling [17]. To address the problem of group effects, Brown, Morrison and Reese [18] was the first to modify the single pile *p-y* curve by introducing a constant reduction factor or p-multiplier. The magnitude of the p-multiplier is always a function of the lateral load or deflection, pile stiffness, pile spacing and soil type [19,20] and is mostly obtained from full-scale field tests on pile groups. Many p-multiplier methods have been developed over time [20–23]. It should be noted that the *p-y* relationship is not a soil property, but rather a pile-soil property. The strain wedge (SW) model initially developed by Norris [24] was introduced to relate stress-strain-strength behaviour in terms of three-dimensional soil-pile interaction, to a one dimensional BEF problem. The SW model has been improved and modified for layered soil [25] and sloping ground [26–28]. Ashour et al. [29] modified the SW model approach to make it applicable for pile groups in layered soils by correcting for the overlap of shear zones, both parallel and normal to the loading direction, among the piles in the group at various depths. The method of Brinch Hansen is often combined with a BEF. The software D-Sheet Piling (for single piles) by Deltares is an example of such a combination wherein the reaction-deformation relationship of the discrete springs is linear elastic with a plastic limit described by the ultimate soil resistance of Brinch Hansen. Typical *p-y* programs are PyPile for single piles and D-Pile Group (MPile) for group piles. Please note that the above-described pile group methods are group equivalent pile procedures, that are based on a subgrade reaction method.

In the second type of models, the soil is represented by an elastic continuum. Poulos [30] described the pile as an infinitely thin linearly elastic strip embedded in an elastic media and approximated the solution numerically. Poulos extended his previous analyses to investigate the influence of a slope on the behaviour of single laterally loaded piles [31]. Apart from single piles, Poulos et al. [32]

Fig. 2. Excavated historical quay wall, 'Maaskade' in Rotterdam. Photograph: Julianus, Eric. "Exposed timber pile foundation of the Maaskade". 2019. Havenbedrijf Rotterdam.

used their previous work on single piles to describe closely spaced lateral loaded pile groups. The application of the principle of minimum potential energy has been applied by Salgado et al. [33] to obtain the response of a laterally loaded pile group in layered elastic soil. Banerjee et al. [34] used the boundary element method to solve the problem of elastic continuum by using two elastic half spaces. Nowadays, 3D FEM (Finite Element Modelling) programs are widely used to solve complex pile-soil-pile interaction problems. Because of the three-dimensional nature of the problem and the high degree of nonlinearity, two-dimensional finite element modelling of laterally loaded piles is fundamentally incorrect. Throughout time, a significant amount of research with 3D FEM modelling for lateral loaded single piles has been carried out. Brown et al. [35] modelled laterally loaded single piles with a numerical three-dimensional finite element model. Other 3D FEM examples are studies that investigate the effect of pile and soil properties [36], the effect of sloping ground [37] and oil-contaminated slopes [38]. Multiple studies [1,39] analysed pile groups subjected to lateral loading using three-dimensional FEM. The effect of a sloping surface on a laterally loaded pile group was researched by Chae et al. [40] using 3D FEM modelling. FEM models require enormous computational effort, which is not proposed for routine design and therefore also certainly not considered suitable for reliability updating.

Therefore, a hybrid method is proposed which strikes a balance between computational speed and modelling accuracy. In this paper, a semi-analytical model for laterally loaded pile groups in layered sloping soil is developed. In the proposed method, the piles are described by a beam on elastic foundation in which the soil behaviour is represented by a series of independent *p-y* springs, idealized with a bilinear elastic-perfect-plastic approximation. This model is earlier developed by Peters [41] and calibrated for single lateral piles in horizontal and gentle sloping sandy and silty soils in the harbour of Rotterdam. The modulus of horizontal subgrade reaction is determined according to the theory of Ménard [42] and the plastic limit is computed with the ultimate soil resistance method of Brinch Hansen [11]. These models, e.g. D-Sheet Piling and Peters, work well for single piles with mild slopes but predictions fail when piles are closely spaced and slope gradients increase. To maintain the advantage of such models, a modification is made by correcting the earth pressure coefficients of Brinch Hansen for each depth. The correction is based on the reduction of the passive soil wedge due to the overlap of shear zones between group piles and the presence of a downward sloping surface. Hereto a new SW model is introduced to construct a three-dimensional soil wedge in layered soil. This proposed SW model takes into consideration the relative sliding of the failure slices within a three-dimensional strain wedge, which is innovative compared to previous studies [25,27–29,43] in which the strain wedge was considered as a whole. Another difference in this study compared to previous work is the way the strain wedge model is used. While in existing SW studies, the strain wedge model is used to obtain the nonlinear *p-y* relations by including the stress-strain-strength relationship into the strain wedge model, in this study the developed wedge model is used as a geometrical tool to obtain correction factors for Brinch Hansen's ultimate soil resistance. The proposed method is therefore an extension of an existing proven pile method making the application widely applicable and computationally fast which is required for use in reliability updating. Furthermore, the method can easily be incorporated in a quay wall model that consists of a framework of elastic beam elements. This model would be suitable to describe failure mechanisms of quay walls concerning lateral pile behaviour both covering structural and geotechnical aspects. Timber creep can be included, using an incremental approach. Apart from historical quay walls, this approach can also be used to model contemporary laterally loaded pile group foundations. First, the methodology of the proposed method is addressed followed by validation with three different experiments. Finally, a discussion and conclusion are provided.

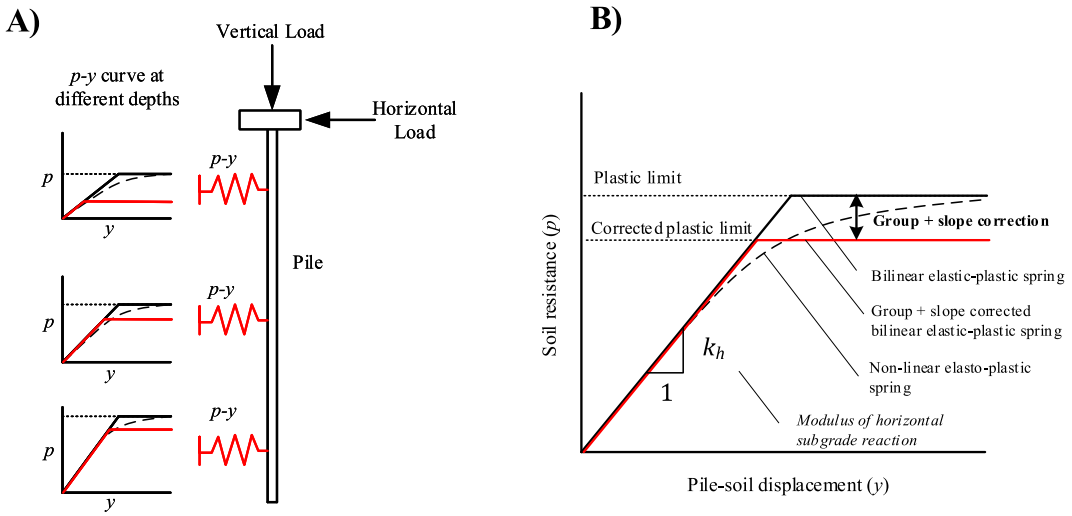

Fig. 3. Schematic representation of proposed BEF method. Pile horizontally supported by *p-y* springs (a). Enlargement of a *p-y* diagram (b). Black dashed line represents a non-linear elastic-plastic *p-y* curve. Black line represents a bilinear *p-y* curve with plastic limit. Red line represents a bilinear elastic *p-y* curve with corrected plastic limit due to pile group and slope surface correction.

2. Methodology

2.1. Beam on elastic foundation using a bilinear approximation

Fig. 3a schematically demonstrates the beam on elastic foundation model (BEF), where the lateral bearing soil-pile interactions are modelled by a series of independent lateral springs (*p-y* spring). In a *p-y* curve, *p* is the soil reaction per unit length of the pile and *y* is the corresponding relative pile-soil displacement. Each individual spring has its own *p-y* curve which is dependent on the soil properties, depth and pile dimensions. While the actual *p-y* curve of foundation soil has a non-linear elastic-plastic character it can, according to API code [44], be idealized with a bilinear elastic-perfect-plastic approximation. The non-linear and bilinear *p-y* curves are schematized in Fig. 3b in black. The gradient of the elastic branch is the modulus of horizontal subgrade reaction, indicated by k_h. In this paper, the horizontal subgrade reaction is determined according to semi-empirical formulas derived by Baguelin et al. [45] in which correlations between geotechnical characteristics of the soil, including the pile dimension, and the Ménard-pressuremeter stiffness were found. These formulas are suitable for soft soils which can be found in the shallow subsurface of Amsterdam. The method developed by Baguelin et al. is one of the many proposed successful methods in which pressuremeter data is used for the design of laterally loaded piles [46–48]. The Ménard stiffness is calculated from the slope of pseudo-elastic pressure-displacement curves and obtained by a series of pressuremeter tests in which a uniform pressure in a cylindrical borehole is gradually increased through an expandable cylindrical probe while measuring the radial expansion. The first stage of the pressure test is recompression followed by a pseudo-elastic soil response which finally becomes plastic. The Ménard stiffness corresponds to the pseudo-elastic soil response. The semi-empirical formulas to obtain the modulus of horizontal subgrade reaction per unit length pile can be found in Appendix A. This subgrade reaction must be multiplied by the width of the pile in order to use it as a spring stiffness ($k = k_h D$) in BEF computations. Furthermore, empirical relations between cone resistance and the Ménard stiffness are provided which can be used in an early design stage. Using a pseudo-elastic soil response over the full pile length is often applied in engineering models [45,49], neglecting that at great pile depths a fully elastic soil response may be a better approach. Despite the absence of a recompression stiffness in the deeper layers, the method is widely used and also incorporated in engineering guidelines like Fascicule 62, A.P.I. and P.H.R.I [50]. The plastic limit is determined with the ultimate soil resistance theory of Brinch Hansen which is further elaborated in section 2.3. To correct for the pile group interaction and the presence of a sloping surface, the plastic limit of individual *p-y* springs is corrected, which can be observed in Fig. 3b with a red solid line. The correction is based on the reduction of the passive soil wedge due to the overlap of shear zones between group piles and the presence of a downward sloping surface. The geometrical shape of the passive soil wedges is modelled with a new proposed strain wedge model for layered soils. It is well established that group interaction effects affect both the ultimate soil resistance and the pile-soil interaction stiffness during the loading trajectory prior to failure. This method does not take

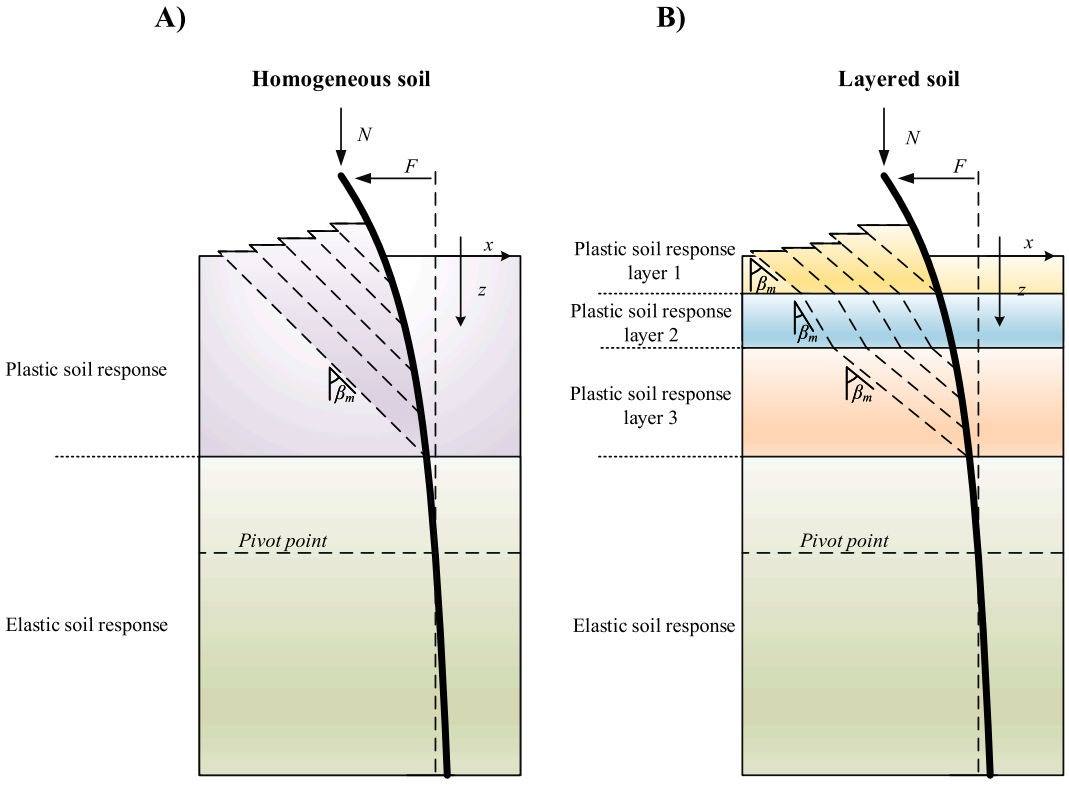

Fig. 4. Development of failure planes for lateral loaded piles in homogeneous (a) and layered (b) soil.

into account a change in horizontal subgrade reaction as a consequence of neighbouring piles and or the presence of a downward directed slope during the loading trajectory. However, as soon as slices of the soil wedges interfere with neighbouring piles a group effect is accounted for in the method. Since the application of this paper is on reliability updating, the ultimate resistance of pile group foundations is of main interest. The lateral failure of pile foundations occurs on average for larger pile group displacements, making this simplification justifiable.

2.2. Proposed strain wedge model

To have consistency between the method of correction and the plastic limit of individual springs, the strain wedge model must be based on the same underlying theory that Brinch Hansen is based on. This theory is the passive Rankine state, developed by Rankine [51]. Rankine's earth pressure assumes a finite amount of failure planes, or as Rankine called planes of rupture, according to the circle of Mohr which is sufficiently correct for reasonably small depths. At greater depths plane case of failure happens horizontally [52]. The strip of soil that is bounded by two failure planes is named a failure slice. A side view of failure slices in front of a laterally loaded pile, located in homogenous soil, is shown in Fig. 4a. For layers that reach their plastic limit, passive failure slices develop towards the surface with mobilized base angle β_m with respect to the vertical, creating a passive wedge in front of the pile. Rankine's theory was developed for an infinite long deflected wall which makes the theory suitable for two-dimensional cases. However, in the situation of a deflected pile, the failure slices which are developed, should be analysed in three dimensions. According to Ashour [29], the passive wedge spreads out with wedge fan angle φ_m. The relation between the mobilized fanning angle and mobilized base angle is formulated in eqn. (1) [25].

$$\beta_m = 45 + \frac{\varphi_m}{2} \tag{1}$$

The shape of the three-dimensional wedge in homogeneous soil is straightforward and evaluated by multiple researchers [10,24,53]. For layered soil, this paper proposes each plastic layer have its own mobilized base angle β_m and wedge fan angle φ_m. A side view of the development of failure slices in layered soil is illustrated in Fig. 4b. Together the failure slices in layered soil form a passive wedge in front of the pile. The geometrical shape of the three-dimensional passive wedge in layered soil is more complex than for homogeneous soil and can be found in Fig. 5. The proposed geometry of the passive wedge is based on the three-dimensional development of failure planes that originate at the axis of the pile at various depths. Because of the complexity of the three-dimensional problem, a discretised approach is applied. The pile is discretised in parts that have a constant height dz. At each discretised depth z of the pile, a failure plane is constructed which develops towards the free surface, intersecting different plastic

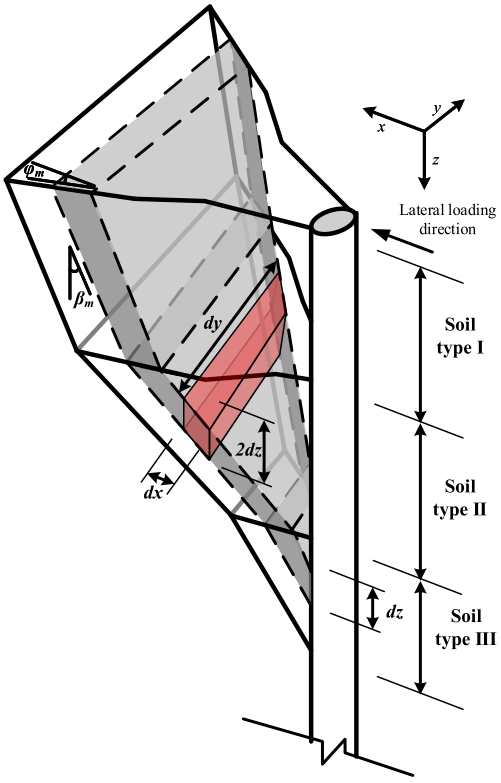

Fig. 5. Proposed three dimensional geometry of passive wedge in layered soil.

layers, with a layer dependent mobilized base angle β_m and mobilized fan angle φ_m. In Fig. 5 indicated in grey, an arbitrary failure slice, bounded by two failure planes, is shown. Each failure slice consists of a number of failure slice cells (FS-cells) of which one is visualized in red in Fig. 5. A fully discretised wedge of an illustrative case can be found in Fig. 8 in which the same colour indication is used as in Fig. 5. The FS-cells are constructed by connecting two superimposed failure planes at each discretised depth. FS-cells therefore have a grid height of 2*dz*, width of *dx* and length of *dy*. Applying this procedure for all failure slices creates a fully discretised wedge which has a stepped structure of cells, e.g. the first failure slice consists of $m = 1$ failure slice cell, the second failure slice consist of $m = 2$ failure slice cells and so on to the deepest plastic failure slice. If for example a laterally loaded pile has a plastic soil response for the first 2.5 m, which is typically found for timber quay wall foundation piles, a total of 25 failure slices is used to describe the wedge in case $dz = 0.1$. The total number of failure slice cells in this particular case is $1 + 2{+}3{+} \ldots {+}25 = 325$. The FS-cells are used to compute the volumetric weight of failure slices and the friction between failure slices at the location of a failure planes. The reduction of both quantities, due to the overlap of shear zones between group piles and the presence of a downward sloping surface, are used to correct the plastic limit of individual *p-y* springs. The volumetric weight of failure slices can be computed with eqn. (2). The friction between failure slices depends on the cohesion of the soil layer and the corresponding surface area of the failure plane and can be computed with eqn. (3).

$$W(z) = \sum_{j=1}^{m} dz_j \times dx_j \times dy_j \times \gamma_j^{'} \tag{2}$$

$$\tau(z) = \sum_{j=1}^{m} \frac{dz_j}{\cos(\beta_{m,j})} dy_j \times c_j^{'} \tag{3}$$

where.

W = total weight of a failure slice, developed at depth z
τ = total friction of a failure plane, developed at depth z
$j = 1{,}2.m$ where m is the amount of FS-cells per failure slice, developed at depth z
γ' = effective weight of FS-cell at depth z
c' = cohesion of FS-cell at depth z
β_m = mobilized base angle at depth z

The integration of equations (2) and (3) takes place over the length of the plastic zone, from the first slice until the last slice, which is equal to the height of the plastic zone divided by grid height *dz*. A balance needs to be found between the grid height and the accuracy of the model outcome. Decreasing the value of *dz* increases the number of failure planes and increases the accuracy of computations on failure plane surface areas and failure slice volumes. However, a fine grid height increases the total number of cells which increases computational effort. As a rule of thumb, halving the grid size *dz* quadruples the total number of failure slice cells needed. To show the impact of the grid height *dz*, a sensitivity study is provided in section 3.1. Based on this study it can be concluded that for piles with a length in the order of L = 12 m, an appropriate grid height is 0.1 m. Assuming that in practice the plastic zone does not become larger than roughly 6 m for 12 m long driven piles, the total amount of grid cells varies globally between 0 and 2000.

Values of the wedge fan angle φ_m have been determined from model tests with a small flat plate in sand. Bowman [54] stated from these model tests that the fan angle is probability a function of the void ratio of the sand, with values ranging from $\varphi'/3$ to $\varphi'/2$ for loose sand to φ' for dense sand. For cohesive soils, assumed to be in an undrained-condition, the value of the internal friction angle φ' is equal to zero and thus the value of the mobilized friction angle φ_m is zero too [11,15,55]. The result is an earth wedge that has a width equal to the width of the pile [14]. This theory is still used by many researchers [43,55,56]. Field tests of Gabr et al. [28] show that the developed soil wedge in clay is in practice wider than the width of the pile and therefore, the volume of this proposed SW model in cohesive soils, according to Reese, could be underestimated. A non-zero fanning angle, to construct the geometrical shape of the passive wedge in undrained cohesive soils, is often applied. Ashour [25,29] assumes a stress-dependent wedge fan angle, according to the Mohr failure criterium. For sand, with a Poisson ratio vary from 0.1 at very small strain to 0.5 or larger (due to dilatancy) at failure, the fanning angle varies from $\varphi_m = 0$ for $\varepsilon = 0$ to for say $\varphi_m = 40°$ at failure. In clay soil with a Poisson's ratio assumed to be 0.5 (undrained behaviour), the fanning angle varies from $\varphi_m = 0$ for $\varepsilon = 0$ to for say $\varphi_m = 25°$ at failure. Kim et al. [57] found a best fit fanning angle of $\varphi'/5$ in cohesive undrained soils based on the comparison between tests results and theoretical force equilibrium.

2.3. Plastic limit reduction

The Brinch Hansen ultimate soil resistance for a laterally loaded single pile, without correction, is given by eqn. (4). This method includes three-dimensional effects, is suitable for layered granular and cohesive soils and is validated with experiments by Christensen [58]. Further elaboration of the mathematical expressions for earth pressure coefficients K_q and K_c in eqn. (4) are given in Appendix B.

$$\sigma_p = K_q \sigma'_v + K_c c \tag{4}$$

where.

σ_p = pressure per unit front area at depth z

σ_v' = effective overburden pressure at depth z
K_q = lateral earth pressure coefficient
K_c = lateral earth pressure coefficient for cohesion
c = cohesion

The resultant earth pressure σ_p, which is the passive minus the active pressure, at depth z is based on the passive Rankine case, in which force equilibrium is found between a resultant pressure force in front of the pile surface area and a friction force of failure slices. The friction force considers the friction between the surface areas of the failure planes (cohesion) and the weight of a failure slices (vertical overburden pressure). The two quantities are multiplied with their corresponding depth depending earth pressure coefficients K_q and K_c to obtain the ultimate soil resistance at depth z. However, these coefficients are based on freely developing failure planes, i.e. freely developed passive wedge, not taking into account surrounding piles or a sloping surface.

Decreasing the spacing between the piles reduces the lateral soil resistance because the soil wedges of the pile group start to interfere [59]. According to Reese et al. [60], the interaction can be distinguished into effects of in-line piles and side-by-side piles. Both interaction effects are due to closely spaced piles, but the type of interaction is different due to the direction of the load. The in-line effects, based on the proposed passive wedge geometry, can be observed in Fig. 6 where the rear pile is located in the 'shadow' zone of the leading pile. The passive wedge in front of the leading pile overlaps with the passive wedge of the rear pile. The mobilized soil of the front pile cannot act as a passive wedge for the rear pile under the assumption that the soil cannot be mobilized twice. Therefore, the overlap between the pile wedges is cut off from the passive wedge of the rear pile. This is indicated in Fig. 6a with a red dashed line. For the side-by-side interaction effect, the piles are organized parallel to the loading direction which is illustrated in Fig. 6b. Again, each pile develops a passive soil wedge and if the pile's wedges overlap, the piles share the same mobilized soil. Under the assumption that the mobilized soil cannot be used twice and that the piles develop the same passive soil wedge, the mobilized soil is divided equally between the piles. The reduction of the middle pile passive wedge is indicated with two red dashed lines.

Piles placed on a downward sloping surface have a smaller resistance compared to piles located in a flat surface because there is less soil available in front of the piles to generate a passive earth wedge [61]. The effect of a sloping surface on a developed passive wedge is visualized in Fig. 6c. The reduction of the passive wedge is indicated with a red dashed line.

To incorporate the effects of closely spaced piles and a downward sloping surface, two depth dependent correction factors are introduced in the Brinch Hansen ultimate soil resistance equation which can be found in eqn. (5).

$$\sigma_{pc} = K_q \Psi_\gamma \sigma_v' + K_c \Psi_c c \tag{5}$$

where.

Ψ_γ = correction factor for the overburden pressure
Ψ_c = correction factor for the cohesion

The correction factors are based on the comparison between a free developing passive wedge with horizontal surface and a corrected passive wedge which takes into account closely spaced piles and a sloping surface. The corrected failure slice weight W_{cpw} and corrected failure plane friction τ_{cpw} are expressed as a fraction of the failure plane weight W and failure plane friction τ of a free developed passive wedge with horizontal surface. These correction factors are depth dependent and can be computed with eqn. (6) and

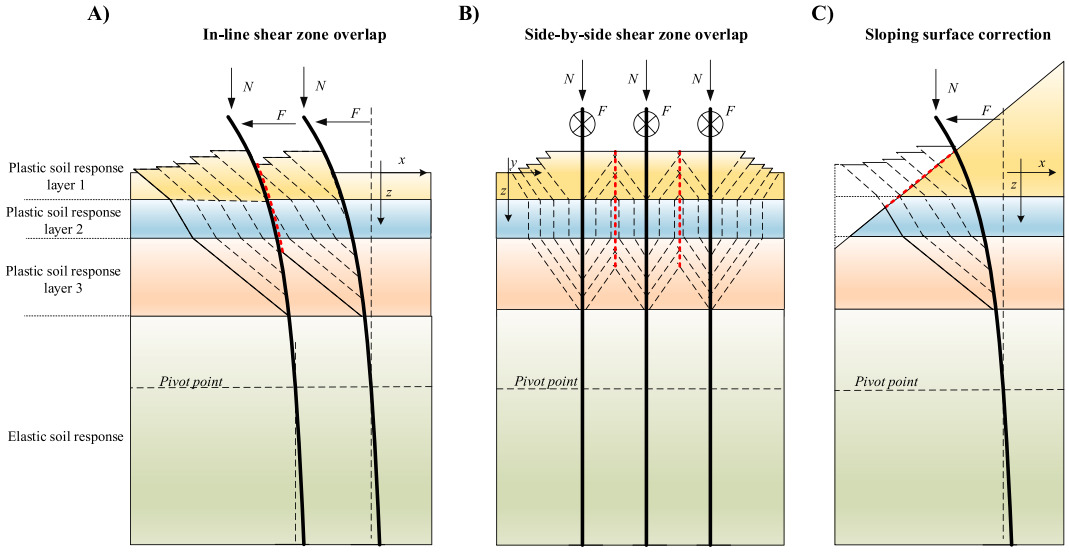

Fig. 6. Correction on the passive wedge based on; in-line shear zone overlap (a), side-by-side shear zone overlap (b), sloping surface correction (c).

eqn. (7). In these equations, the subscript *cpw* stands for 'corrected passive wedge', which is the trimmed volumetric shape of a passive single pile wedge due to the presents of closely spaced piles and or a sloping surface.

$$\Psi_\gamma(z) = 1 - \frac{W - W_{cpw}}{W} = \frac{W_{cpw}}{W} \tag{6}$$

$$\Psi_c(z) = 1 - \frac{\tau - \tau_{cpw}}{\tau} = \frac{\tau_{cpw}}{\tau} \tag{7}$$

The weight W_{cpw} and friction τ_{cpw} of a corrected passive wedge are computed with eqn. (2) and eqn. (3) which is the same procedure as for a free developed passive wedge. However, FS-cells can be narrowed in width, separated into two parts or completely removed from the passive wedge due to; in-line effects, side-by-side effects, a sloping surface or a combination of the three. The three-dimensional geometrical shape of a corrected passive wedge in layered soil can be found in Fig. 7. The passive wedge is similar to the wedge illustrated in Fig. 5. However, this illustrative figure shows the in-line effect on the rear pile wedge. In green, an FS-cell within a failure plane is shown which is separated into two parts. In case of a separated cell, an effective length for *dy* is used which is the sum of two cell parts with length *dy/2*. The correction on the pressure coefficient for cohesion is assumed to be proportional to the friction reduction between failure slices within the passive wedge.

2.4. Computational example plastic limit reduction

To illustrate the method which is used to correct the plastic limit of bilinear springs, a brief example is given. This example shows the in-line, side-by-side and sloping surface effect on the plastic limit of *p-y* springs. Let us consider a laterally loaded pile with length L = 12 m and typical diameter $D = 0.324$ m. It is assumed that the first 2 m of soil exceeds the plastic strain limit, due to lateral deformations, and hence a passive wedge, with wedge depth $h = 2$ m, is formed in front of the pile. Three soil layers are present of which the properties are summarized in Table 1. For demonstrative purposes, the fanning angle φ_m is taken equal to the internal friction angle φ' for each layer.

First, the free developed passive wedge is constructed. The geometry is presented in Fig. 8 in which 8a shows the side view of the passive wedge and 8b the three-dimensional development of the passive wedge. For visualization purposes, this geometrical shape is constructed with a grid height of $dz = 0.2$ m. At each discretised depth of the pile, a failure plane is constructed towards the surface with mobilized base angle β_m. FS-cells are constructed by connecting all superimposed failure planes at each discretised depth. At a larger distance from the pile, the cell length *dy* increases due to the wedge fan angle φ_m. Further computations are done with a refined

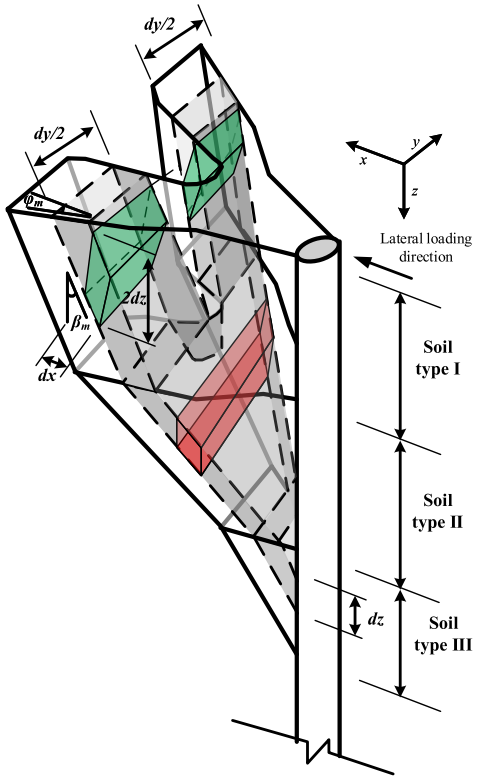

Fig. 7. Geometry of passive wedge after correction for in-line shear zone overlap. The leading pile and its passive wedge causes a 'cut-out' in the passive wedge of the rear pile.

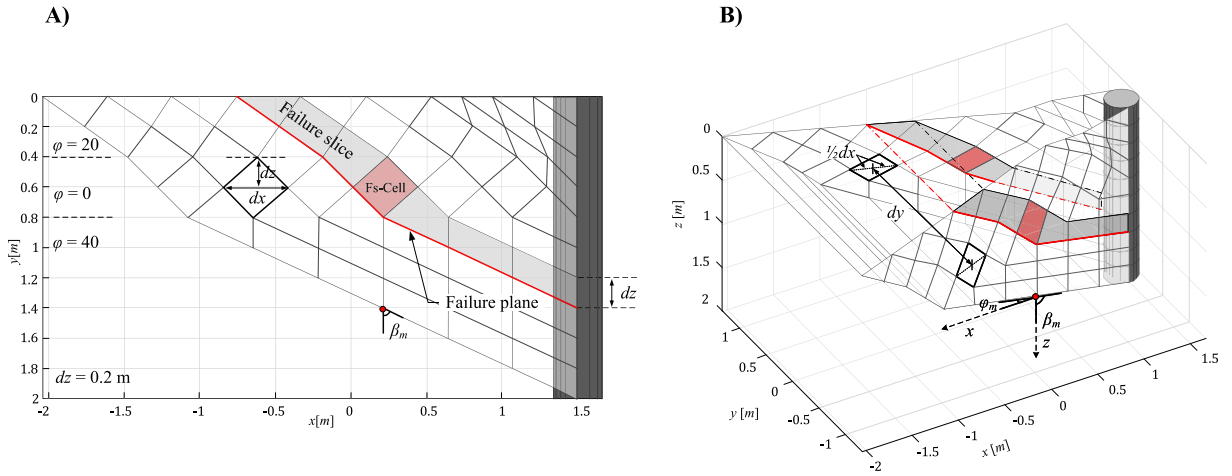

Fig. 8. Geometrical shape of passive wedge in illustrative example. Side view (a), three-dimensional view (b).

Table 1
Layer properties illustrative example.

Layer	Depth [m]	φ' [deg]	c' [kN/m^2]	γ' [kN/m^3]
1	0.0–0.4	20	0	18
2	0.4–0.8	0	20	17
3	0.8–10	40	0	18

grid height $dz = 0.05$ m to make computations more accurate. The passive wedge, containing all developed failure slices, is visualized in Fig. 9a. To illustrate the correction method the following cases are addressed.

a) In-line effect; leading pile with similar pile wedge is located 1.5 m in front of the rear pile.
b) Side-by-side effect; neighbour piles with similar pile wedges are located 1.0 m next to the middle pile.
c) Sloping surface effect; a slope inclination of 1V:3H is considered.

The corrected three-dimensional geometrical shape of each case is visualized in Fig. 9b,c,d. Comparing the freely developed passive wedge from Fig. 9a with the corrected passive wedges in Fig. 9b,c,d results in a corrected Brinch Hansen ultimate resistance, which is used as a plastic limit to the *p-y* springs in the BEF method. For each case, the plastic limit and its correction are plotted for each discretised depth in Fig. 10. Please note that only the first 2 m of the pile is plotted because this part exceeds the plastic limit. For all plastified soil layers a 3rd degree polynomial fit $f(z)$ is made which is used to describe the corrected plastic limit as a continuous function of depth. These continuous functions are used to analytically solve the BEF problem of which the solution method is given in section 2.5. As can be seen in Fig. 10a, the failure slices up to 1 m depth, are not affected by the presence of the leading pile wedge. This corresponds also to Fig. 9b. At a depth greater than 1 m, the failure slices are reduced in volume because of the presence of the leading pile passive wedge. The effect is the reduction of ultimate soil resistance for the failure slices which are formed at the lowest part of the passive wedge. Because the passive wedge of the leading pile has a kinked shape, a kink can be observed in the plot at around 1.4 m. For the side-by-side effect case, which can be observed in Fig. 10b, the reduction of the ultimate soil resistance starts at depths larger than 1.2 m. Like the previous case, the volume of the deeper failure slices is reduced due to the presence of the passive wedges of the neighbouring piles. In the last case, the effect of the slope is discussed. As can be seen in Fig. 10c, the ultimate soil resistance is reduced for the top and bottom layers. However, the middle layer is not affected by the presence of the slope. According to Brinch Hansen, the cohesive layer only has passive resistance due to cohesion between the failure slices which in this case are not affected by the slope geometry. As a result, the cohesive FS-cells from failure planes that developed in the cohesive layer, weren't affected or cropped out. This causes the ultimate soil resistance by Brinch Hansen not to be reduced for the middle layer. In case the cohesive layer was the top layer, a noticeable effect would be observed.

2.5. Analytical solution BEF problem

The differential equation of a single beam on elastic Winkler foundation is presented in eqn. (8) [62] and its solution and application for laterally loaded piles has been discussed by a number of authors [63,64] and is still widely used. In eqn. (8), x is the displacement, EI *is* the flexural rigidity of the beam, k is the stiffness of the elastic foundation and q is an arbitrary distributed load that is dependent on the depth z.

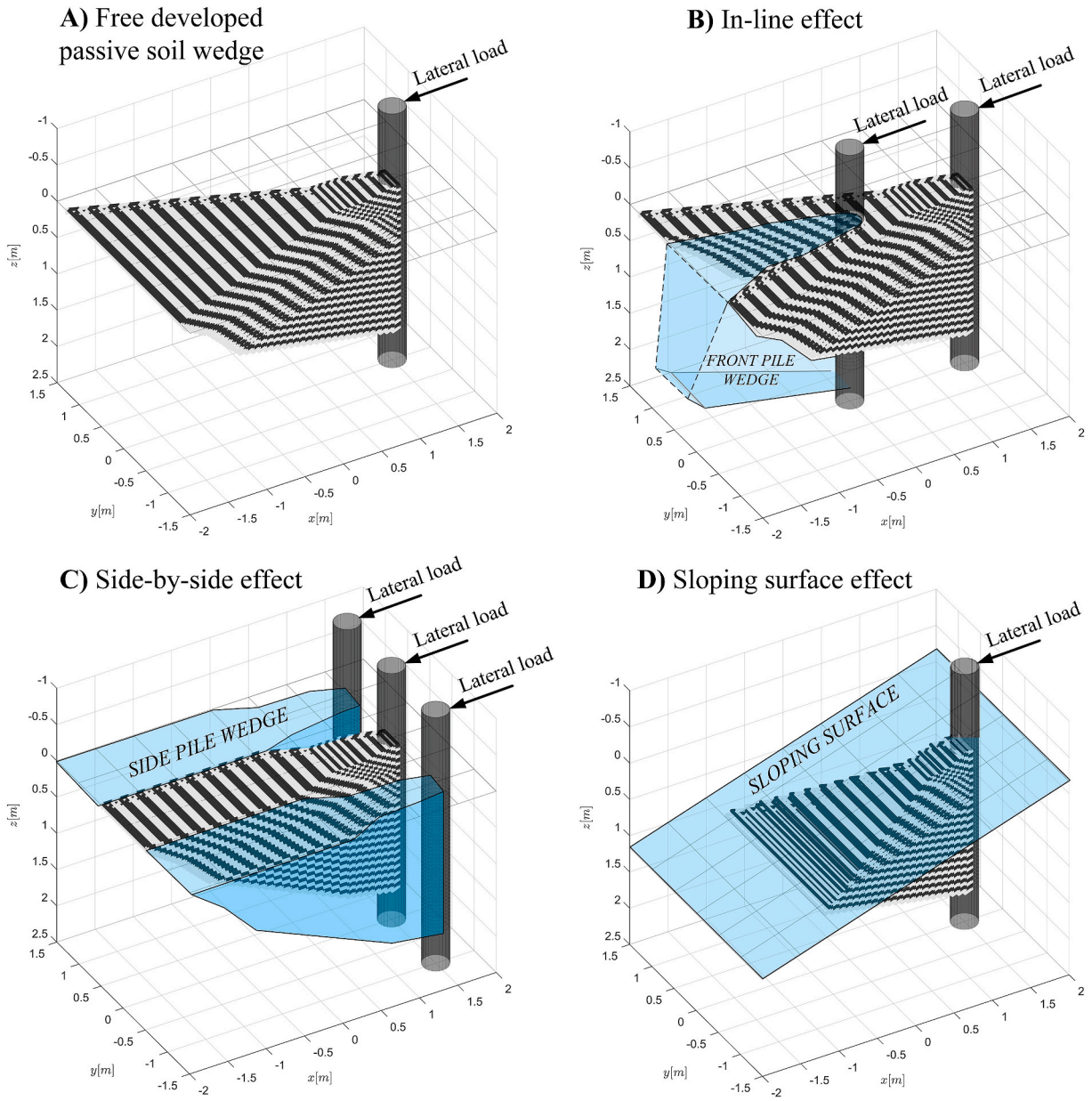

Fig. 9. Three-dimensional geometrical shape of passive wedge in which failure planes are indicated with a black-white pattern (a). Correction of the passive soil wedge due to in-line shear zone overlap (b), due to side-by-side shear zone overlap (c), and due to a sloping surface (d). Loading on the pile is slope downward directed.

$$EI\frac{d^4x(z)}{dz^4} + kx(z) = q(z) \tag{8}$$

Each layer of soil has its own modulus of subgrade reaction k of which the plastic limit is varying with depth. A soil layer that reaches the plastic limit becomes independent of the lateral pile displacement and can therefore be modelled as a constant distributed load. A distinction between plastic and elastic layers must be made in order to solve the BEF problem analytically. An analytical solution is preferred because it reduces the computational time and provides a good insight into the fundamentals of the problem. The bending of a pile in layered soil, subjected to a lateral load F, is described by multiple beams on elastic foundation, of which the general form can be found in eqn. (9). Here, $i = 1,2..n$ where n represents the number of unique soil layers, i.e. if the subsurface around the pile consists of a sand layer and a clay layer of which part of that clay layer reaches the plastic limit, three unique soil layers are present. Please note that an extra term is added to eqn. (9) which includes the effect of the axial load on the bending of the pile. A schematic parameter visualization is provided in Fig. 11. The top of the pile is indicated by z_1 and the tip of the pile is indicated by z_{n+1}. The depth

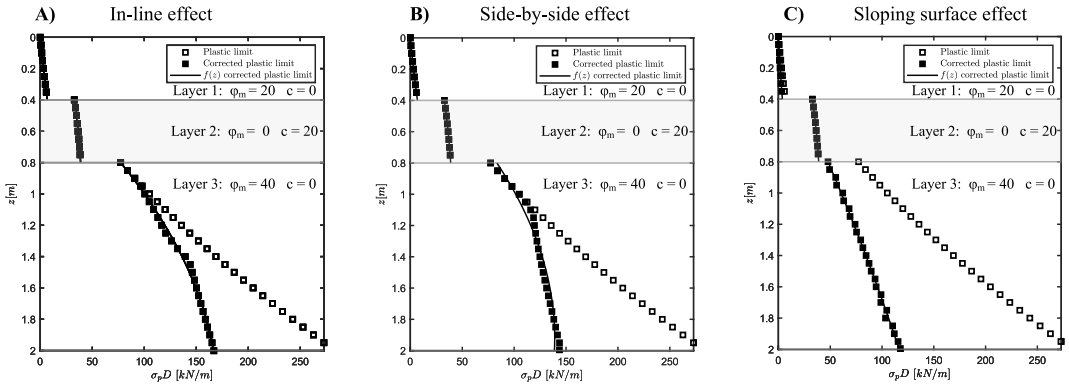

Fig. 10. Correction plastic limit due to in-line shear zone overlap (a), due to side-by-side shear zone overlap (b), and due to a sloping surface (c).

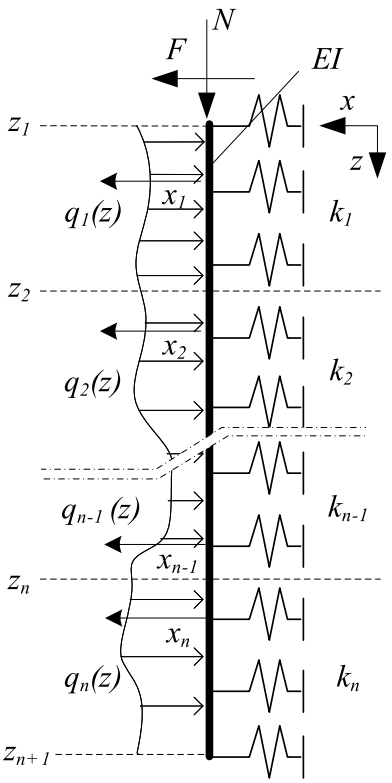

Fig. 11. Parameter overview of BEM method.

at which interfaces between unique soil layers are present is indicated by z_2, z_3.. z_n. The depth of unique soil layers, and thus also the thickness of each layer, is taken as a multiple of the grid height dz in order to avoid coupling problems between the proposed strain wedge method and the BEF method.

$$EI\frac{d^4x_i(z)}{dz^4} + N\frac{d^2x_i(z)}{dz^2} + k_i x_i(z) = q_i(z) \quad i = 1, 2..n \tag{9}$$

In eqn. (9), x is the lateral pile displacement, EI the flexural rigidity of the pile, N the axial load, z the depth, $k = k_h D$, the stiffness of the elastic foundation and $q(z)$ the depth dependent distributed load to describe fully plastified layers. For the depth dependent distributed load, the corrected plastic limit is used so that $q_i(z) = f_i(z) = a_i z^3 + b_i z^2 + c_i z + d_i$. Here, $f(z)$ is the polynomial function that describes the corrected plastic limit $\sigma_{pc}D$ as function of depth which is elaborated in section 2.4. The polynomial function is chosen to the third order which makes it possible to find a simple particular solution in the form q/k for the general differential equation presented in eqn. (9). With higher orders, particular solutions become more complex for this problem [65]. For $N < 2\sqrt{kEI}$, the general solution to eqn. (9), for each unique soil layer i, is formulated in eqn. (10). The solution is written with natural exponential

functions which gives computational advantages over trigonometric functions.

$$x_i(z) = C_{(4i-3)}e^{z\sqrt{\left(-\frac{\sqrt{N^2-4\,EI\,k_i}}{EI}-\frac{N}{EI}\right)}} + C_{(4i-2)}e^{-z\sqrt{\left(-\frac{\sqrt{N^2-4\,EI\,k_i}}{EI}-\frac{N}{EI}\right)}} + C_{(4i-1)}e^{z\sqrt{\left(\frac{\sqrt{N^2-4\,EI\,k_i}}{EI}-\frac{N}{EI}\right)}} + C_{4i}e^{-z\sqrt{\left(\frac{\sqrt{N^2-4\,EI\,k_i}}{EI}-\frac{N}{EI}\right)}} + \frac{6\,N\,a_i\,z}{k_i^{\,2}} + \frac{2\,N\,b_i}{k_i^{\,2}} - \frac{a_i z^3}{k_i} - \frac{b_i z^2}{k_i} - \frac{c_i z}{k_i} - \frac{d_i}{k_i}\;;\; i = 1, 2..n \tag{10}$$

Where C_1,C_2, …C_{4n-1}, C_{4n} are the integration constants to be determined from the boundary and interface conditions. In total $4 \bullet n$ integration constants need to be solved. It should be noted that for an existent mathematical solution N needs to be smaller than $2\sqrt{kEI}$ and thus k needs to be given a non-zero value, even for fully plastified soil layers. When elaborating the boundary and interface conditions the following relations are used, presented in eqn. (11). Here, φ is the pile rotation, M the moment and V the shear force.

$$\varphi = -\frac{dx(z)}{dz}, M = -EI\frac{d^2x(z)}{dz^2}, V = -EI\frac{d^3x(z)}{dz^3} \tag{11}$$

The four boundary conditions, two at the top and two at the bottom of the pile, are denoted in eqn. (12) to eqn. (15). It should be noted that the boundary conditions at the top of the pile, can be adapted in case a displacement or external moment is imposed. For now, a lateral load is considered. The horizontal component of the axial load needs to be included in the shear boundary condition. Especially with large deflections, this second order effect works progressive and cannot be neglected.

$$M(z = z_1) = -EI\frac{d^2x_1(z_1)}{dz^2} = 0 \tag{12}$$

$$V(z = z_1) = -EI\frac{d^3x_1(z_1)}{dz^3} = F - \frac{dx_1(z_1)}{dz}N \tag{13}$$

$$M(z = z_{n+1}) = -EI\frac{d^2x_n(z_{n+1})}{dz^2} = 0 \tag{14}$$

$$V(z = z_{n+1}) = -EI\frac{d^3x_n(z_{n+1})}{dz^3} = 0 \tag{15}$$

In case the pile has a constant flexural rigidity EI over the full pile length, the interface conditions between the different unique layers can be written as follows in eqn. (16) to eqn. (19). The interface conditions are based on the continuity of displacement, slope, moment and shear force.

$$x_{i-1}(z_i) = x_i(z_i) \quad i = 2,\ 3..n \tag{16}$$

$$\frac{dx_{i-1}(z_i)}{dz} = \frac{dx_i(z_i)}{dz} \quad i = 2,\ 3..n \tag{17}$$

$$\frac{d^2x_{i-1}(z_i)}{dz^2} = \frac{d^2x_i(z_i)}{dz^2} \quad i = 2,\ 3..n \tag{18}$$

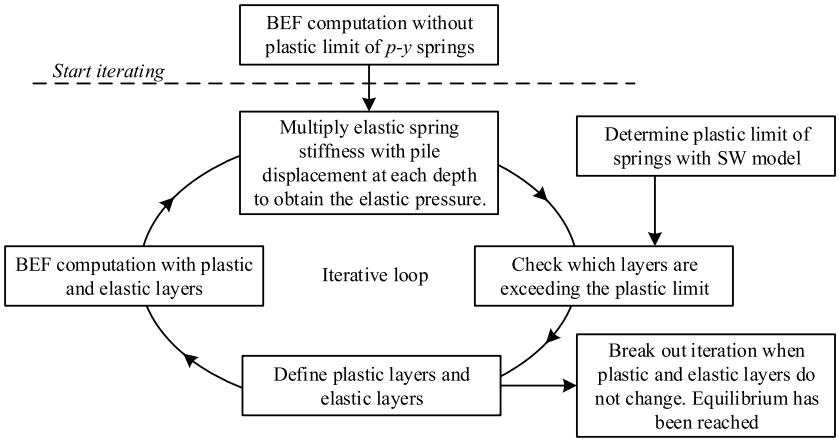

Fig. 12. Flowchart of iterative solution to solve the non-linear BEF problem.

$$\frac{d^3x_{i-1}(z_i)}{dz^3} = \frac{d^3x_i(z_i)}{dz^3} \quad i = 2,\ 3..n \tag{19}$$

The general solution described in eqn. (10) is substituted into the boundary and interface conditions which gives a linear system of equations. Aligning the coefficients of each integration constant in columns results in a coefficient matrix A. The matrix of variables, which is a vector containing all unknown integration constants, is constructed and named C. The remaining terms, i.e. terms that do not contain integration constants, are used to form a force vector Q. Solving the linear system $AC = Q$, shown in eqn. (20), returns the value of all integration constants. Substituting the integration constants back into the general solution, presented in eqn. (10), results in the displacement distribution $x(z)$ of the entire laterally loaded pile.

$$AC = Q \text{ where } \quad A = \begin{bmatrix} A_{1,1} & A_{1,2} & \cdots & A_{1,4n} \\ A_{2,1} & A_{2,2} & \cdots & A_{2,4n} \\ \vdots & \vdots & \ddots & \vdots \\ A_{4n,1} & A_{4n,2} & \cdots & A_{4n,4n} \end{bmatrix}, \quad Q = \begin{bmatrix} Q_1 \\ Q_2 \\ .. \\ Q_{4n} \end{bmatrix}, \quad C = \begin{bmatrix} C_1 \\ C_2 \\ .. \\ C_{4n} \end{bmatrix} \tag{20}$$

In practice it is not known in advance which soil layers develop full plasticity because this depends on the deflection of the pile, which is unknown prior to the calculation. Therefore, an iterative process is required in which equilibrium is sought between the lateral load on the pile cap and the resistance that elastic and fully plastic soil layers cause. A flow chart of this iterative process is given in Fig. 12. First, a fully elastic computation without plastic *p-y* branch is performed which results in the displacement of the pile. At each discretised depth *dz*, the displacement is multiplied with its elastic spring stiffness to obtain the elastic pressures. At each discretised depth *dz*, plastic and elastic soil responses are identified. Accordingly, a new 'unique layering' distribution is made with elastic and plastic layers which is used for a new BEF computation. This iterative process is repeated until the layering distribution does not change or becomes repetitive. Since the thickness of each unique layer is chosen to be a multiple of the grid height *dz* fewer iteration steps are needed with larger grid size. The downside is a decrease in modelling accuracy, which is elaborated in section 3.1. Once equilibrium is found, the rotation, moment and shear force distributions of the laterally loaded pile can be obtained with eqn. (11).

3. Results of validation

Based on the analytical model presented in this paper, a computer program has been developed in MATLAB to solve the problem of a laterally loaded pile within a pile group, located in layered sloping soil. To demonstrate the capability of the model, a comparison of field test results versus model results is made. The field tests have their own characteristic set-up and different soil and pile properties, making it possible to validate all model applications. These are: laterally loaded pile groups in layered soil [66], lateral loaded single piles in layered sloping soil [67] and lateral loaded single pile at various distances near a slope crest in sand [38].

3.1. Full-scale lateral-load tests of a 3 × 5 pile group in soft clays and silts (snyder, J. L. 2004)

Snyder conducted a series of static lateral load tests on a group of fifteen piles arranged in a 3 × 5 pattern. The side-by-side spacing was 1.07 m and the in-line spacing was 1.27 m. The piles with diameter $D = 0.324$ m, pile length $L = 12$ m and row average flexural rigidity $EI = 25{,}000$ kNm^2 were loaded at $z = -0.5$ m. An isolated single pile test was executed for comparison purposes. The flexural rigidity of the single pile is $EI = 28{,}600$ kNm^2. Cohesive layers are normally consolidated giving $c = su$ and $\varphi = 0$. As an initial estimate, the wedge fan angle φ_m is assumed to be equal to the friction angle which results in a wedge fan angle of zero for all clay layers. The model is calibrated on the single pile and on the pile group load test. The layers and their engineering properties are summed in Table 2.

In Fig. 13, the bending moment distribution of the lateral loaded single pile is plotted for a range of imposed pile displacements. The maximum moment for 4, 6 and 13 mm is slightly underestimated. For the other imposed displacements, the predicted moment distribution fits the measured results very well. The depth of the predicted moment occurs at progressively deeper depths with increased deflections, corresponding to the measurements. For all deflections, the depth of the zero-moment crossing is on average 0.5 m lower than in the measurements. In Fig. 14 the moment distributions for the leading pile row and trailing pile rows are plotted. Because the in-line and side-by side effects for all trailing pile rows is the same, model predictions for pile rows 2–5 have identical force distributions. The measurements for the second pile row are used to validate the model predictions on the rear pile rows. The maximum

Table 2
Engineering properties full scale 3 × 5 pile group experiment (Snyder, 2004).

Depth [m]	γ' [kN/m^3]	Sort [−]	q_c [kPa]	c [kN/m^2]	φ [deg]
0–1.2	9.05	clay	1000	20	0
1.2–2.1	9.05	clay	1000	35	0
2.1–3.0	9.05	clay	1000	20	0
3.0–4.8	8.14	sand	15,000	0	38
4.8–5.3	9.05	clay	5000	56.9	0
5.3–5.9	9.05	clay	1000	25	0
5.9–6.4	9.0	clay	4000	54	0
6.4–20	8.14	sand	10,000	0	33

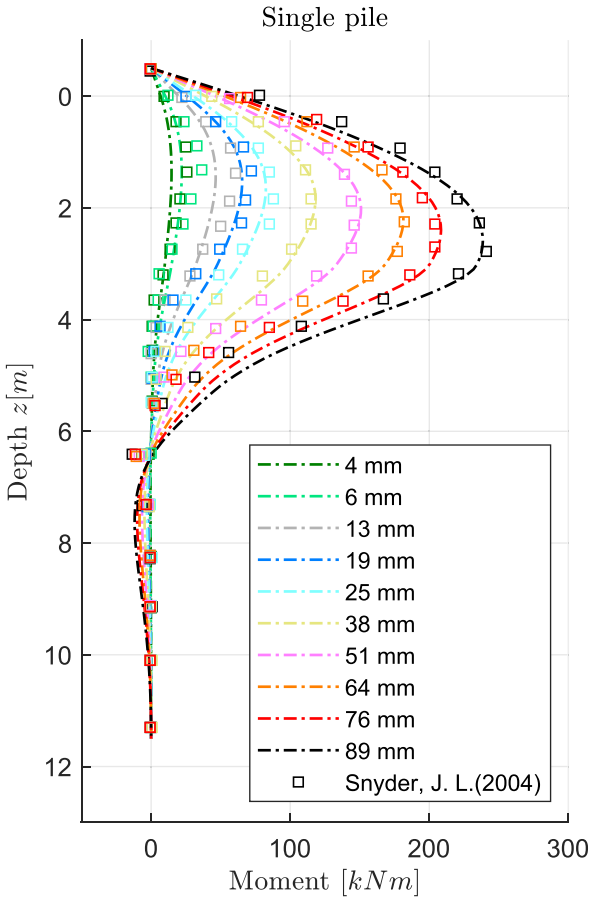

Fig. 13. Bending moment distribution of lateral loaded single pile for imposed pile deflections as function of depth.

moment of all pile rows is underestimated for the deflections 6 and 13 mm. For the largest deflection (89 mm), the model overpredicts the moment by 10%. For all other deflections, the moment prediction is very accurate. The zero-moment crossing corresponds to the measured data. For deflections larger than 38 mm, the model predicts larger maximum moments for the leading pile row compared to the maximum moments in the rear pile rows. This is in accordance with the measured results. The shape of the moment distributions is predicted well, the trailing pile row moment distributions stretch out more into the depth compared to the leading pile row.

In Fig. 15, the average leading and trailing pile rows loads are plotted as function of the pile group deflection. In Fig. 16, the maximum moment of the leading and trailing pile is plotted as function of the pile group deflection. In both figures, single pile model predictions and measured data is provided. The wedge fan angle φ_m for cohesive layers is calibrated on the lateral load and bending moment data which results in the best fit for a wedge fan angle of 15°. To show the sensitivity of the fanning angle, an upper and lower limit of 10° is presented which results in a bandwidth of 5–25° for the cohesive layers. The chosen bandwidth corresponds to the theoretical limit which was found by Ashour, described in section 2.2. It can be observed that the wedge fan angle has much more impact on the trailing rows than the leading rows which is logical since the leading piles do not have in-line interactions. The initial estimate, in which the wedge fan angle φ_m is assumed to be equal to the friction angle, overestimates (especially for larger deflections) the lateral loads and moments by roughly 10–20% for the trailing pile rows. Because the first 3 m of soil is cohesive with a wedge fan angle of zero, in-line and side-by-side pile interactions are small causing an underestimated reduction of the plastic limit. To increase the interaction effects, a non-zero wedge fan angle is assigned to the cohesive layers. A non-zero wedge fan angle corresponds to the shear cracks that appeared in the cohesive top layers during the field experiment.

First, the force-displacement predictions in Fig. 15 are discussed. The model prediction for the single pile fits the measured data perfectly. Also, the leading pile row prediction is very accurate. The force-displacement curve of the leading pile row is predicted slightly lower than the curve of the single pile due to side-by-side interaction. This is also in good agreement with the measurements. Because the in-line and side-by side effects for all trailing pile rows is the same, model predictions for pile rows 2–5 have identical force distributions. However, in the experiment, the force-displacement curves of all pile rows are presented. The spread of these curves is quite large, row 2 and 4 have a steeper curve than row 3 and 5. As mentioned before, the model is not capable of making distinctions between the different trailing pile rows.

In the first stage of loading, group deflections are underestimated. For large lateral group loads, near geotechnical failure, group deflections are overestimated (e.g. a steeper force-displacement curve in the first stage of loading and more gentle force-displacement

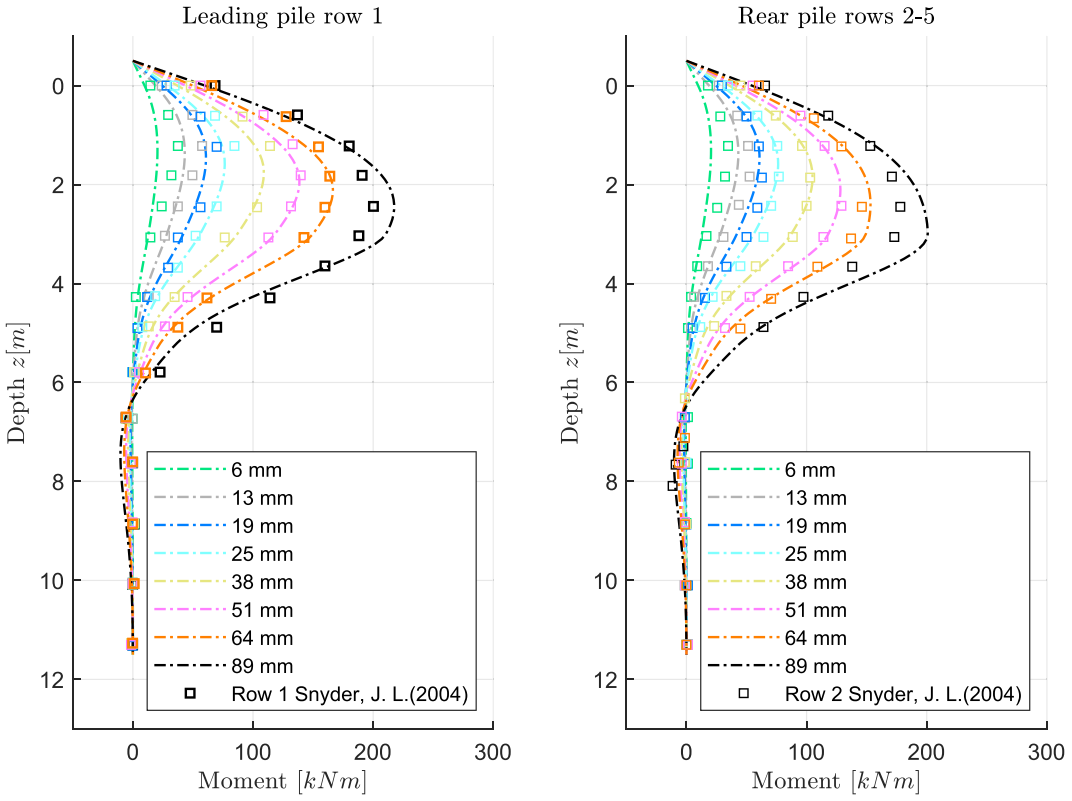

Fig. 14. Bending moment distribution of lateral loaded 3×5 pile group for imposed pile deflections as function of depth. Left plot considers leading pile row, right plot considers the trailing pile rows 2–5. To validate the trailing pile rows, field data of pile row 2 is used.

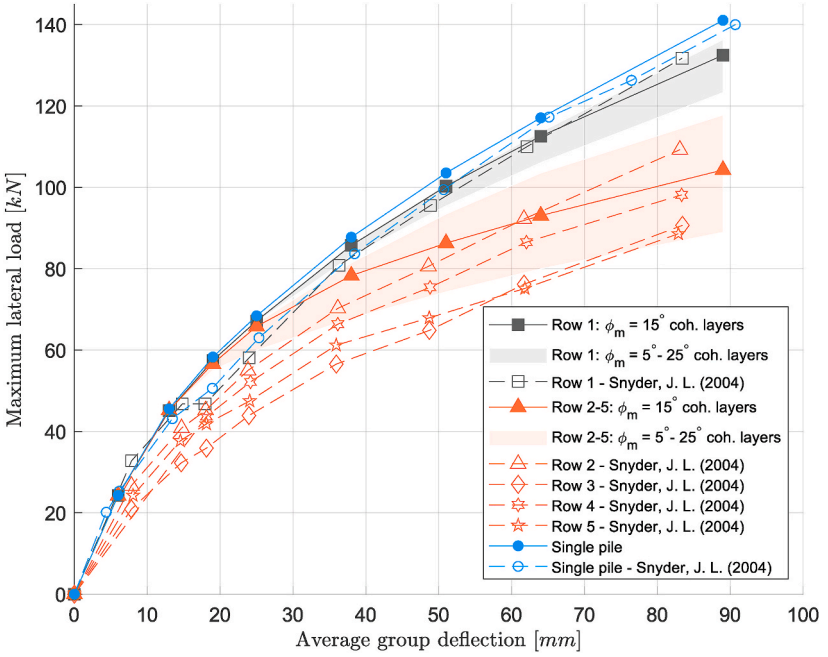

Fig. 15. Comparison of average pile row load vs. applied group deflection. Pile group is computed with $\varphi_m = \varphi$ for granular layers and $\varphi_m = 15$ deg. for cohesive layers with a bandwidth of ±10 deg.

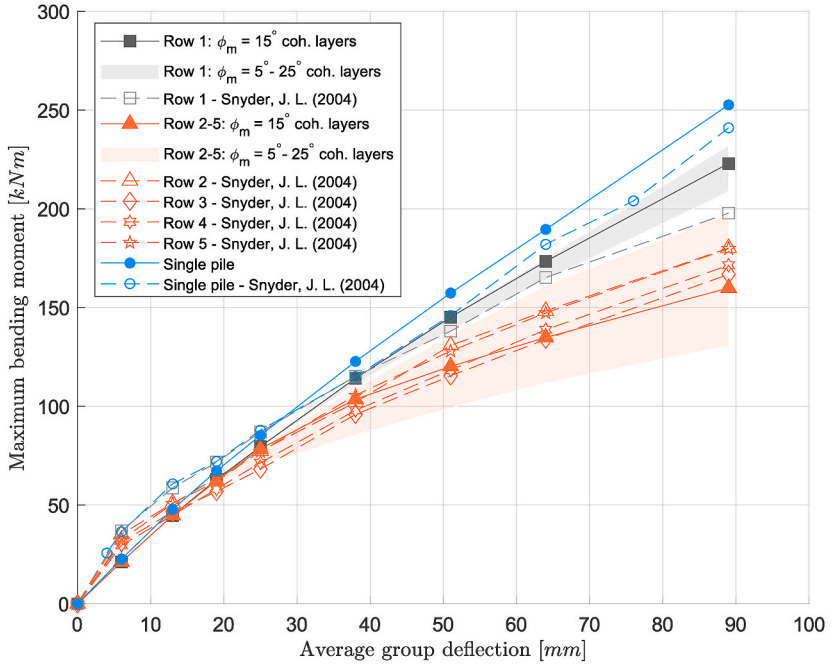

Fig. 16. Comparison of maximum bending moment vs. average group deflection. Pile group is computed with $\varphi_m = \varphi$ for granular layers and $\varphi_m =$ 15 deg. for cohesive layers with a bandwidth of ±10 deg.

curve at the final loading stage). This effect can be explained. Passive wedges start to grow as function of the pile deflection and start to interfere with each other at a certain displacement. According to this method, it is not possible to have group interaction for small displacements since the passive wedges are still small in volume at that moment of time. Also, the compacting of soil between the piles in case of large pile group deflections is not taken into account. The compacted soil cannot escape between the piles creating a higher stiffness of the soil. Despite these two effects, the model is capable of predicting the average lateral load of the trailing rows, especially for the larger displacements, quite well.

Subsequently, the moment-displacement prediction in Fig. 16 is discussed. The model prediction for the single pile fits the measured data perfectly. Also, the leading pile row prediction is accurate, only for the largest deflection of 89 mm an error of approximately 10% is made. It should be noted that this measured moment is an outlier in the dataset of Snyder. Again, the moment-displacement curve of the leading pile row is predicted slightly lower that the curve of the single pile due to side-by-side interaction. Because the in-line and side-by side effects for all rear pile rows is the same, model predictions for pile rows 2–5 have identical moment

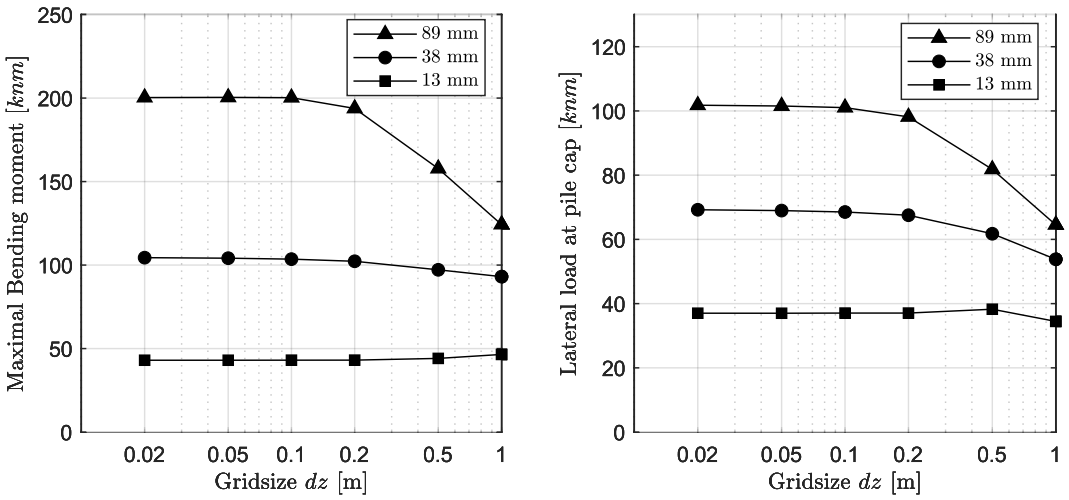

Fig. 17. Sensitivity of grid height *dz* on model outcome. Left figure indicates bending moment predictions for three imposed deflections as function of *dz*. Right figure indicates the lateral load at the pile cap for three imposed deflections as function of *dz*.

distributions. The spread in maximum measured moment of the trailing pile rows is less compared to the spread found in the force-displacement measurements. The maximum moment prediction by the model is very accurate and pretty much the average of the trailing pile row measurements. Also, the pile group displacement at which group interaction start to take place is predicted perfectly.

Computations in this section are performed with a grid height of $dz = 0.05$ m. To illustrate the effect of the grid height dz on the accuracy on the model outcome, the maximal bending moment and lateral load at the pile cap are plotted as function of dz for three different imposed pile cap displacements 13 mm, 38 mm and 89 mm. The results can be found in Fig. 17. It can be observed that for smaller grid sizes than $dz = 0.1$ m, the model outcome does not change and accuracy doesn't improve further. An appropriate pile height to grid height ratio, without losing accuracy, in this validation is $L/dz = 120$.

From the calibration with the Snyder experiment it can be concluded that our model is able to predict lateral loads and bending moment magnitudes at all levels for the leading and the trailing piles in the pile group very accurately, which is a sign that the soil pressure distributions applied in the model are correct.

3.2. Lateral resistance of piles at the crest of slopes in sand (mirzoyan, A. D. 2007)

Mirzoyan conducted a series of static lateral load tests on a single pile in layered horizontal and in sloping soil. The slope in the field test has an inclination of 1V:1.75H which is rather steep for underwater slopes but still in the range of application for canal bed slopes in Amsterdam. The field tests are executed at the same location as the field test of Snyder. The piles have a diameter $D = 0.324$ m, pile length $L = 13.5$ m flexural rigidity $EI = 28{,}600$ kN m^2 and are loaded at $z = -0.5$ m. The layers and their engineering properties are summarized in Table 3. Cohesive layers are normally consolidated giving $c = su$ and $\varphi = 0$.

In Fig. 18, force-displacement diagrams are shown for the single pile in layered horizontal and sloping soil. In Fig. 19, the maximum bending moment as function of the lateral load is presented. The first 3 m of soil is classified as sand with slight cohesion in which a passive wedge develops. The wedge fan angle φ_m is calibrated on the lateral load and bending moment data which results in a best fit for a wedge fan angle of 20°. According to Bowman [54], the wedge fan angle in sand varies with values ranging from $\varphi'/3$ to $\varphi'/2$ for loose sand up to φ' for dense sand. The calibrated wedge fan angle of 20° corresponds to a value of $\varphi'/2$ which can be classified as moderated loose to slightly dense sand. During the field experiment, shear cracks appeared at the surface, with an angle of 22° with respect to the loading direction. The best fit wedge fan angle of 20° is in very good agreement with the angle of shear cracks found in the field experiment. The force-displacement model prediction of the pile with a horizontal soil surface matches the measurements very well. For the pile in sloping soil, above 150 kN lateral load, the model predicts larger displacements than measured. The bending moment prediction fits the measured data for both horizontal and sloping surface very well. To show the sensitivity of the fanning angle on the lateral resistance and bending moment, an upper and lower limit of 20° is presented which results in a bandwidth of 0–40°. The chosen bandwidth corresponds to the theoretical limits found by Ashour [25] and the maximum wedge fan angle in dense sand according to Bowman [54]. Increasing the wedge fan angle causes larger reductions of the plastic limit of p-y springs which decreases the lateral loads resistance and thus bending moments. Reducing the wedge fan angle has an opposite effect, smaller plastic limit reductions cause larger lateral resistance and larger bending moments.

The theoretical lower limit, a zero wedge fan angle, found by Ashour [25] is only valid for cases with no strain. Therefore, a wedge fan angle of zero at failure in sand is impossible and meaningless. Small wedge fan angles can underpredict the plastic limit reduction and lead to an overprediction of the lateral resistance of piles in sloping soil. However, with large fanning angles, bending moments can be underestimated.

From the calibration on the Mirzoyan experiment it can be concluded that our model is able to predict lateral loads and bending moment magnitudes at all levels for piles in sloping soil with high accuracy. The correct match of the bending moment indicates that the lateral soil resistance prediction is correct. The less accurate match of the displacement means that there might be an underestimated effect in the model of the reduced soil stiffness in the case of sloping soils.

3.3. Experimental and numerical studies of laterally loaded piles located near oil-contaminated sand slope (abdelhalim et al., 2020)

Abdelhalim et al. performed small scale experiments on a laterally loaded pile in sandy soil near the crest of a slope. The following model parameters were used; pile diameter $D = 0.021$ m, pile length $L = 0.4$ m, loading point $z = -0.05$ m, slope = 1V:2H, flexural

Table 3
Engineering properties full scale lateral single pile test (Mirzoyan, 2007).

Depth [m]	γ' [kN/m^3]	Sort [−]	q_c [kPa]	c [kN/m^2]	φ [deg]
0.0–1.8	17.0	sand	15,000	6	45
1.8–2.7	6.9	sand	7500	6	45
2.7–3.0	9.13	clay	2000	40	0
3.0–3.6	9.13	clay	2000	50	0
3.6–4.8	9.13	clay	2000	40	0
4.8–6.3	8.3	sand	15,000	0	38
6.3–6.8	9.13	clay	2000	56	0
6.8–7.5	9.13	clay	2000	25	0
7.5–7.9	9.13	clay	2000	54	0
7.9–20	9.13	sand	15,000	0	47

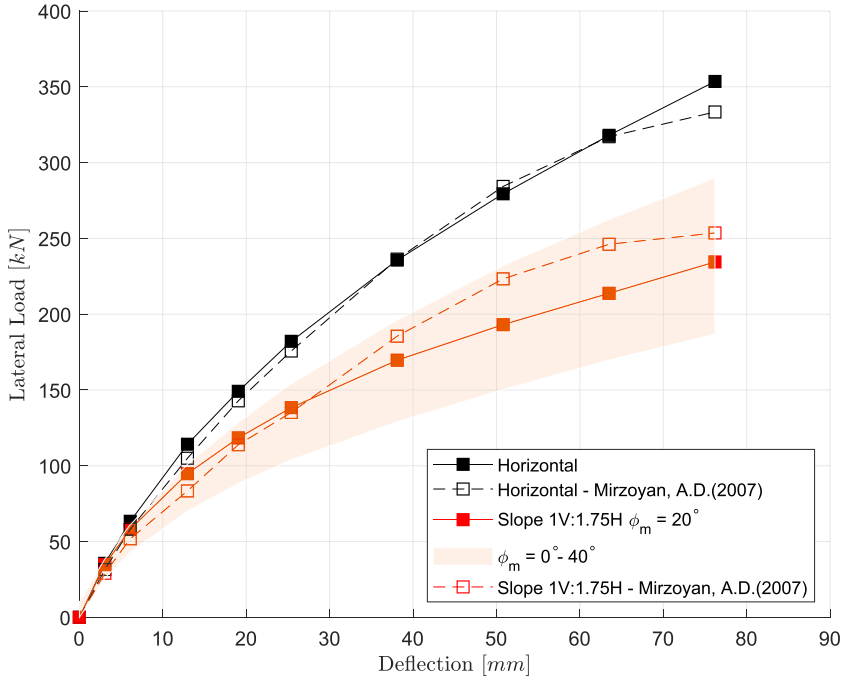

Fig. 18. Comparison of maximal bending moment vs applied load for a single pile in horizontal and sloping ground.

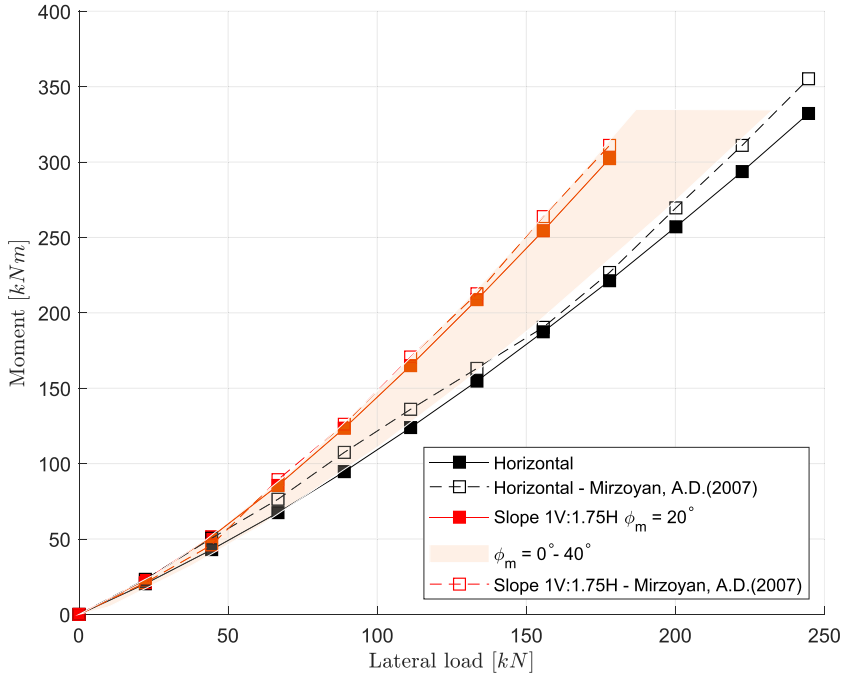

Fig. 19. Comparison of pile load vs applied pile deflection for a single pile in horizontal and sloping ground.

Table 4
Soil properties small scale pile near slope experiment.

Depth [m]	γ' [kN/m^3]	Sort [–]	q_c [kPa]	c [kN/m^2]	φ [deg]
0–1.0	17	sand	350	1.2	37

rigidity $EI = 183$ kN•m2. In the experiment, the distance X near the slope is varied from 'at the crest' to 8D from the crest. First, the model is calibrated on the $X = 8D$ force-displacement data which most closely resembles a pile loaded in horizontal surface. The engineering properties are summarized in Table 4.

For the X = 8D case, the plastic limit correction due to the slope is small and therefore, the magnitude of the wedge fan angle has a limited impact on the lateral resistance of the pile. For the case in which the pile is located on the crest of the slope, plastic limit corrections are the largest and therefore, the wedge fan angle φ_m is calibrated on the X = 'at crest' force-displacement data. A best fit is found for a wedge fan angle of 21° which, according to Bowman [54], corresponds to medium to dense sand ($\varphi'/2 < \varphi_m < \varphi'$). The wedge fan angle is estimated to be 20–35° based on shear crack formation during the experiment. The calibrated wedge fan angle is in the same range as the angle of the shear cracks during the experiment. For the cases, X = 8D, 6D, 4D, 2D and 'at the crest' the force-displacement diagram is presented in Fig. 20. The model predictions are compared with the measured data. For X = 8D, 6D, 2D and 'at crest' the model predictions match the data very well. For X = 4D, the displacements are overpredicted by approximately 10%. Fig. 20 visualizes the softening behaviour of the different cases at a distance X near the crest of a slope. For all cases, the model predicts a slightly steeper force-displacement curve between 50 N and 170 N lateral load.

From the calibration on the Abdelhalim et al. experiment, it can be concluded that our model is able to predict lateral loads for piles at a distance X near the crest of a sloping soil with high accuracy.

4. Discussion

Our model is able to predict pile forces and displacements with high accuracy for three different field experiments. With a relatively low number of parameters, a proper estimate of the pile behaviour can be made. The computational time is fast, enabling applications such as trend analyses and probabilistic calculations. Single pile computations with a horizontal surface in layered granular and cohesive soil can be executed with high precision. For pile group computations, pile row interactions can be modelled in good agreement with the field experiment of Snyder [66]. However, for the pile group computation two main findings are discussed based on the results of the validation:

1) To model the interaction between group piles in undrained cohesive soils, a non-zero fanning angle needs to be applied. For plastic limit computations with Brinch Hansen, the effective friction angle in undrained cohesive layers needs to be taken zero [11]. Because the effective friction angle and mobilized fanning angle are related to each other, this results in a fanning angle equal to zero. The construction of a passive wedge without fanning angle results in a narrow wedge width and steep base angle causing the passive wedge to be rather small in volume. The side-by-side and in-line overlapping of shear zones becomes small to negligible which gives almost no plastic limit reduction of *p-y* springs. In order to increase the in-line and side-by-side effect of the trailing pile rows in the model, the wedge fanning angle for undrained cohesive layers should be given a non-zero value. Note that the effective friction angle should not be increased as an attempt to increase the wedge fan angle and thus the shear zone overlapping. This would result in an increase of the plastic limit of *p-y* springs and as a result in a decrease of the difference between leading and trailing piles and in an overall larger resistance of the pile group, which are both incorrect.
2) In the first stage of loading, group deflections are underestimated. For large lateral group loads, near geotechnical failure, group deflections are overestimated (e.g. a steeper force-displacement curve in the first stage of loading and more gentle force-displacement curve at the final loading stage). The same trend, but to a lesser extent, can be observed for the moment prediction. The following phenomena not included in the model may play a role here:

- Passive wedges start to grow as function of the pile deflection and start to interfere with each other at a certain displacement. The moment at which interaction starts to take place has to do with the pile group configuration, strength of piles and the soil characteristics. According to this method, it is not possible to have group interaction for small displacements since the passive wedges are still small in volume at that moment of time. This underestimates the group deflection and therefor also bending moments for small lateral group loads.
- The soil-pile-soil interaction is captured by a volume based passive wedge reduction. However, soils get compacted between the piles when the pile group deflects, causing an increase in soil stiffness and extra loads on piles (e.g. the trailing pile row pushes its soil against the leading pile row). For large group deflections, the soil stiffness could be underestimated. As a result, group deflections due to large lateral loads can be overestimated.

The model seems to work well for sloping surfaces despite the fact that the effect of a slope on the overburden pressure is not taken into account. The overburden pressure σ_p is computed by multiplying the depth with the effective weight of soil layers as if the surface is horizontal. Effective soil pressures below a slope or near the crest of a slope are smaller than effective soil pressures that are computed for a horizontal surface. The result is a stiffer predicted soil pile response, especially for the first stage of loading. This effect can be seen in both slope experiments. This paper only prescribes a slope correction method for slope downward loaded piles. In the situation of slope inward loaded piles, the wedge failure slices become larger due to the 'extra' soil compared to a flat surface resulting in a higher ultimate soil resistance. Correction factors are now larger than 1 instead of smaller.

The following phenomena are not included in the model and have a limited to neglectable effect; Increase of friction between soil and pile, in case of excessive pile deformation, is not evaluated as contributor to lateral resistance and has only a noticeable effect for large diameter piles. Furthermore, the gap behind the pile is not taken into account, which reduces the active pressure in the top layers. Also, soil accumulation in front of piles due to excessive pile deflections, causing an increase of the lateral resistance, is not part of the model.

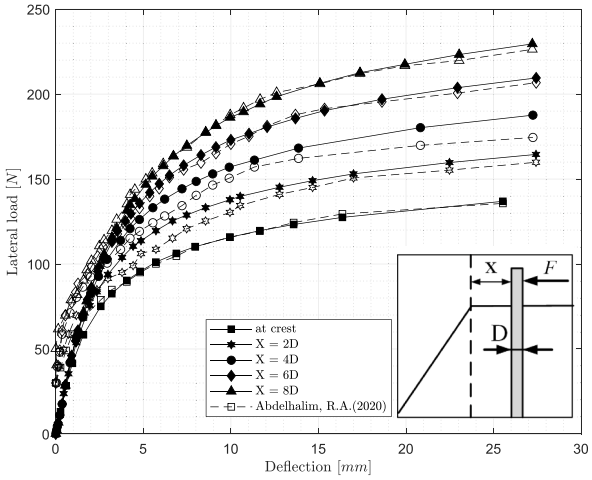

Fig. 20. Comparison of pile load vs. applied deflection for various distances X with respect to the slope crest.

5. Conclusion

A semi-analytical model is proposed as analysis tool for laterally loaded pile groups. The model is validated with three different field experiments. The lateral loaded pile, as a part of a pile group in layered sloping soil, is modelled as a BEF. The elastic subgrade reaction of the soil is described by *p-y* springs which have a depth-dependent bilinear elastic-perfect-plastic approximation. The plastic limit is corrected based on the reduction of the passive soil wedge due to the overlap of shear zones with other piles at close proximity and due to the presence of a soil slope, going downward in the direction of the lateral load.

The model predicts displacement, force and bending moment distributions in good agreement with a variety of field experiments. However, for pile groups, the maximum bending moments as function of the group displacement in the trailing pile rows could be underestimated, especially when the pile is near geotechnical failure. For piles located in a slope or near the crest of a slope, the model is an accurate and powerful tool to use. The accuracy of the model and its predictive value is affected by an informed choice of parameters, amongst which the fanning angle of the passive wedge, as discussed in the paper. For each experiment, a best fit fanning angle is calibrated for the top layers in which the passive earth wedge forms. For the Snyder field experiment, a 15° fanning angle is found for undrained cohesive clay layers, corresponding to the non-zero fanning angle in undrained cohesive soils found by Ashour et al. [25,29] and Gabr et al. [28]. The Mirzoyan field experiment and the Abdelhalim et al. experiment are exectuted in moderate dense sand with slight cohesion and for both experiments, a best fit fanning angle equal to $\varphi'/2$ is found. This dependency on the friction angle correspond to the observed shear cracks at the surface during the experiments and to theoretical values stated by Bowman [54]. Because the fanning angle is very much dependent on the soil characteristics a large variety of fanning angles can be found in literature (see section 2.2). This makes it is hard to choose an appropriate estimation without doing any experiments prior to performing computations. It is therefore recommended to perform field tests and geotechnical research in order to calibrate computational models. Together with the TU Delft, Amsterdam develops a large field experiment on quay walls and groups of quay wall foundation piles to calibrate computational models such as the model elaborated in this paper.

For conservative pile design, a large wedge fan angle is recommended in the determination of the lateral pile capacity while for bending moment predictions, a small wedge fan angle is advised. The model has a short computational time, in the order of seconds, compared to complex three-dimensional FEM software, in the order of minutes to hours, which makes it an excellent tool for preliminary pile design and probabilistic analysis. With relatively little input, a proper estimate of the pile behaviour can be made.

Declaration of competing interest

The authors declare that they have no known competing financial interests or personal relationships that could have appeared to influence the work reported in this paper.

Appendix A. Ménard modulus of subgrade reaction

$$\frac{1}{k_h} = \begin{cases} \dfrac{1}{3E_m}\left[1.3R_0\left(2.65\dfrac{R}{R_0}\right)^{\alpha} + \alpha R\right] \\ \dfrac{2R}{E_m} \times \dfrac{4(2.65)^{\alpha} + 3\alpha}{18} \; if \; R \geq R_0 \end{cases} \quad \text{if} \;\; R \geq R_0 \tag{A1}$$

where.

k_h = is the modulus of horizontal subgrade reaction [kN/m^2]
E_m = is the pressiometric modulus [kN/m^2]
R_0 = is a constant: $R_0 = 0.3$ [m]
R = half the diameter of the pile [m]
ɑ is the rheological coefficient which depends on the soil type (See Table A1).

Table A1
Values of rheological coefficient ɑ.

	Peat	Clay	Loam	Sand	Gravel
Over consolidated	–	1	2/3	1/2	1/3
Normally consolidated	1	2/3	1/2	1/3	1/4
Decomposed, weathered		1/2	1/2	1/3	1/4

The pressiometric modulus E_m can be obtained via correlations with the cone resistance q_c.

Peat: $E_m = 3.5\ q_c$
Clay: $E_m = 2.5\ q_c$
Loam: $E_m = 1.5\ q_c$
Sand: $E_m = 0.85\ q_c$
Gravel: $E_m = 0.6\ q_c$

Appendix B. Brinch Hansen ultimate soil resistance

$$K_q = \frac{K_q^0 + K_q^\infty \times \alpha_q \times \frac{z}{D}}{1 + \alpha_q \times \frac{z}{D}} \tag{B1}$$

$$K_c = \frac{K_c^0 + K_C^\infty \times \alpha_c \times \frac{z}{D}}{1 + \alpha_c \times \frac{z}{D}} \tag{B2}$$

where

$$K_q^0 = e^{\left(\frac{\pi}{2} + \varphi\right) \times \tan\varphi} \times \cos\varphi \times \tan\left(\frac{\pi}{4} + \frac{\varphi}{2}\right) - e^{\left(-\frac{\pi}{2} + \varphi\right) \times \tan\varphi} \times \cos\varphi \times \tan\left(\frac{\pi}{4} - \frac{\varphi}{2}\right)$$

$$K_c^0 = \left[e^{\left(\frac{\pi}{2} + \varphi\right) \times \tan\varphi} \times \cos\varphi \times \tan\left(\frac{\pi}{4} + \frac{\varphi}{2}\right) - 1 \right] \times \cot\varphi$$

$$K_q^\infty = K_c^\infty \times K_c^\infty \times \tan\varphi$$

$$K_c^\infty = N_c d_c^\infty$$

$$d_c^\infty = 1.58 + 4.09 \times \tan^4\varphi$$

$$N_c = \left[e^{\pi \times \tan\varphi} \times \tan^2\left(\frac{\pi}{4} + \frac{\varphi}{2}\right) - 1 \right] \times \cot\varphi$$

$$K_0 = 1 - \sin(\varphi)\ for\ OCR = 1$$

$$\alpha_q = \frac{K_q^0}{K_q^\infty - K_q^0} \times \frac{K_0 \times \sin\varphi}{\sin\left(\frac{\pi}{4} + \frac{\varphi}{2}\right)}$$

$$\alpha_c = \frac{K_c^0}{K_c^\infty - K_c^0} \times 2\sin\left(\frac{\pi}{4} + \frac{\varphi}{2}\right)$$

References

[1] Selby AR, Arta MR. Three-dimensional finite element analysis of pile groups under lateral loading. Comput Struct 1991;40:1329–36.
[2] Dong J, Li Z, Lu P, Jia Q, Wang G, Li G. Design ice load for piles subjected to ice impact. Cold Reg Sci Technol 2012;71:34–43.
[3] Han Y, Vaziri H. Dynamic response of pile groups under lateral loading. Soil Dynam Earthq Eng 1992;11:87–99.
[4] Klaassen RKWM, Creemers JGM. Wooden foundation piles and its underestimated relevance for cultural heritage. J Cult Herit 2012;13:S123–8.
[5] Klaassen RKWM. Bacterial decay in wooden foundation piles—patterns and causes: a study of historical pile foundations in The Netherlands. Int Biodeterior Biodegrad 2008;61:45–60.
[6] Korff M, Hemel MJ, Peters DJ. Collapse of the Grimburgwal, a historic quay in Amsterdam. Proc Inst Civil Eng-Forensic Eng 2022:1–8.
[7] Amsterdam G. Actieplan bruggen en kademuren. Amsterdam; 2019.
[8] Straub D. Reliability updating with equality information. Probabilist Eng Mech 2011;26:254–8.
[9] Ehre M, Papaioannou I, Straub D. Efficient conditional reliability updating with sequential importance sampling. In: Proceedings in applied Mathematics and Mechanics; 2018.
[10] Blum H. Wirtschaftliche dalbenformen und deren berechnung. Verlag nicht ermittelbar; 1932.
[11] Hansen JB. The ultimate resistance of rigid piles against transversal forces. Danish Geotech Institute Bulletin 1961;12:1–9.
[12] Sun K. Laterally loaded piles in elastic media. Journal of Geotechnical Engineering 1994;120:1324–44.
[13] Broms BB. Lateral resistance of piles in cohesionless soils. J Soil Mech Found Div 1964;90:123–56.
[14] Matlock H. Correlations for design of laterally loaded piles in soft clay. Offshore technology in civil engineering's hall of fame papers from the early years. 1970. p. 77–94.
[15] Reese LC, Cox WR, Koop FD. Field testing and analysis of laterally loaded piles om stiff clay. Offshore Technology Conference; 1975.
[16] Jeanjean P. Re-assessment of py curves for soft clays from centrifuge testing and finite element modeling. Offshore Technology Conference; 2009.
[17] Bransby MF. Selection of p–y curves for the design of single laterally loaded piles. Int J Numer Anal Methods GeoMech 1999;23:1909–26.
[18] Brown DA, Morrison C, Reese LC. Lateral load behavior of pile group in sand. Journal of Geotechnical Engineering 1988;114:1261–76.
[19] Rollins KM, Peterson KT, Weaver TJ. Lateral load behavior of full-scale pile group in clay. Journal of geotechnical and geoenvironmental engineering 1998;124:468–78.
[20] McVay M, Casper R, Shang T-I. Lateral response of three-row groups in loose to dense sands at 3D and 5D pile spacing. Journal of Geotechnical Engineering 1995;121:436–41.
[21] Duncan JM, Robinette MD, Mokwa RL. Analysis of laterally loaded pile groups with partial pile head fixity. Advances in Designing and Testing Deep Foundations: in Memory of Michael W O'Neill 2005. p. 235-250.
[22] Ruesta PF, Townsend FC. Evaluation of laterally loaded pile group at Roosevelt Bridge. J Geotech Geoenviron Eng 1997;123:1153–61.
[23] McVay M, Zhang L, Molnit T, Lai P. Centrifuge testing of large laterally loaded pile groups in sands. J Geotech Geoenviron Eng 1998;124:1016–26.
[24] Norris GM. Theoretically based BEF laterally loaded pile analysis. Navtes; 1986. p. 361–86.
[25] Ashour M, Norris G, Pilling P. Lateral loading of a pile in layered soil using the strain wedge model. Journal of geotechnical and geoenvironmental engineering 1998;124:303–15.
[26] Xu L-Y, Cai F, Wang G-X, Ugai K. Nonlinear analysis of laterally loaded single piles in sand using modified strain wedge model. Comput Geotech 2013;51:60–71.
[27] Peng W, Zhao M, Xiao Y, Yang C, Zhao H. Analysis of laterally loaded piles in sloping ground using a modified strain wedge model. Comput Geotech 2019;107:163–75.
[28] Gabr MA, Borden RH. Lateral analysis of piers constructed on slopes. Journal of geotechnical engineering 1990;116:1831–50.
[29] Ashour M, Pilling P, Norris G. Lateral behavior of pile groups in layered soils. J Geotech Geoenviron Eng 2004;130:580–92.
[30] Poulos HG. Behavior of laterally loaded piles I. Single Piles. Journal of Soil Mechanics & Foundations Div; 1971.
[31] Poulos HG. Behaviour of laterally loaded piles near a cut or slope. Aust Geomech J 1976;6.
[32] Poulos HG, Davis EH. Pile foundation analysis and design. 1980.
[33] Salgado R, Tehrani FS, Prezzi M. Analysis of laterally loaded pile groups in multilayered elastic soil. Comput Geotech 2014;62:136–53.
[34] Banerjee PK, Davies TG. The behaviour of axially and laterally loaded single piles embedded in nonhomogeneous soils. Geotechnique 1978;28:309–26.
[35] Brown DA, Shie C-F. Three dimensional finite element model of laterally loaded piles. Comput Geotech 1990;10:59–79.
[36] Fan C-C, Long JH. Assessment of existing methods for predicting soil response of laterally loaded piles in sand. Comput Geotech 2005;32:274–89.
[37] Ng CWW, Zhang LM. Three-dimensional analysis of performance of laterally loaded sleeved piles in sloping ground. J Geotech Geoenviron Eng 2001;127:499–509.
[38] Abdelhalim RA, El Sawwaf M, Nasr AM, Farouk A. Experimental and numerical studies of laterally loaded piles located near oil-contaminated sand slope. Engineering Science and Technology, an International Journal 2020;23:744–57.
[39] Brown DA, Shie C-F. Numerical experiments into group effects on the response of piles to lateral loading. Comput Geotech 1990;10:211–30.
[40] Chae KS, Ugai K, Wakai A. Lateral resistance of short single piles and pile groups located near slopes. Int J GeoMech 2004;4:93–103.
[41] Peters DJ. New analytical plasticity model for lateral loaded mono-piles. -; 2022 (Paper in writing).
[42] Ménard L, Bourdon G, Gambin M. Methode generale de calcul d'un rideau ou d'un pieu sollicite horizontalement en fonction des resultats pressiometriques. Sols Soils 1971;6.
[43] Yang M, Deng B, Wang Y. A simplified calculation method for the near-slope laterally loaded pile based on a passive wedge model. Adv Civ Eng 2019;2019.
[44] American Petroleum I. Recommended practice for planning, designing, and constructing fixed offshore platforms. American Petroleum Institute; 1989.
[45] Baguelin F, Jézéquel J. Etude experimentale du comportement de pieux sollicites horizontalement. Ann Itbtp-serie sols et fondations- 1972;91.
[46] Briaud JL, Smith T, Meyer B. Using the pressuremeter curve to design laterally loaded piles. In: Offshore Technology Conference. OnePetro; 1983.
[47] Robertson PK, Hughes JM, Campanella RG, Brown P, McKeown S. Design of laterally loaded piles using the pressuremeter. The pressuremeter and its marine applications: second International Symposium. ASTM International; 1985.
[48] Baguelin F. Rules for the structural design of foundations based on the selfboring pressuremeter test. Symp on the Pressuremeter and its Marine Application. IFP, Paris. 1982. p. 347–62.
[49] Briaud J-L. Geotechnical engineering: unsaturated and saturated soils. John Wiley & Sons; 2013.
[50] Maouche H. Analyse numerique de la reponse non lineaire d'un pieu sous sollicitations laterales.
[51] Rankine WJM. II. On the stability of loose earth. Philosophical transactions of the Royal Society of London; 1857. p. 9–27.
[52] Hansen JB, Lundgren H. Hauptprobleme der Bodenmechanik. Springer-Verlag; 1960.
[53] Reese LC. Behavior of piles and pile groups under lateral load. 1986. p. 276. Report No FHWA/RD-85/106.
[54] Bowman ER. Investigation of the lateral resistance to movement of a plate in cohesionless soil. 1958.
[55] Stacul S, Squeglia N. Analysis method for laterally loaded pile groups using an advanced modeling of reinforced concrete sections. Materials 2018;11:300.
[56] Lin C, Han J, Bennett C, Parsons RL. Analysis of laterally loaded piles in soft clay considering scour-hole dimensions. Ocean Eng 2016;111:461–70.
[57] Kim Y, Jeong S, Lee S. Wedge failure analysis of soil resistance on laterally loaded piles in clay. Journal of Geotechnical and geoenvironmental engineering 2011;137:678–94.
[58] Christensen NH. Model tests with transversally loaded rigid piles in sand. Danish Geotech Ins. Bull Copenhagen 1961:10–6.
[59] Wright SG. Laterally loaded pile groups. Preprints for Short Course on Deep Foundations 1982:1–20.
[60] Reese LC, Van Impe WF. Single piles and pile groups under lateral loading. CRC press; 2010.
[61] Mezazigh S, Levacher D. Laterally loaded piles in sand: slope effect on py reaction curves. Can Geotech J 1998;35:433–41.
[62] Winkler E. Die Lehre von der Elasticitaet und Festigkeit: mit besonderer Rücksicht auf ihre Anwendung in der Technik für polytechnische Schulen, Bauakademien, Ingenieue, Maschinenbauer, Architecten, etc. Dominicus; 1867.

[63] Gleser SM. Lateral load tests on vertical fixed-head and free-head piles. 1953. p. 75–101.
[64] Reese LC. Non-dimensional solutions for laterally loaded piles with soil modulus assumed proportional to depth. 1956.
[65] Simone A. An introduction to the analysis of Slender structures. TU Delft; 2007.
[66] Snyder JL. Full-scale lateral-load tests of a 3x5 pile group in soft clays and silts. 2004.
[67] Mirzoyan AD. Lateral resistance of piles at the crest of slopes in sand. 2007.